# APPLICATIONS OF ACTIVATED IRON MEDIA SYSTEM FOR REMOVAL OF ANTIMONY FROM WATER

A Thesis

by

JAEYOUNG CHOI

Submitted to the Office of Graduate and Professional Studies of
Texas A&M University
in partial fulfillment of the requirements for the degree of

MASTER OF SCIENCE

| | |
|---|---|
| Chair of Committee, | Xingmao Ma |
| Co-Chair of Committee, | Yongheng Huang |
| Committee Members, | Kuang-An Chang |
| Head of Department, | Robin Autenrieth |

December 2018

Major Subject: Civil Engineering

# ABSTRACT

Antimony (Sb) is an element in the group XV that has allotropic modifications and two main oxidation states as Sb(III) and Sb(V) in nature. Antimony is a pollutant of concern for its carcinogenic and bioaccumulation effects. Sb presence in drinking water or wastewater is strictly regulated worldwide. Removing Sb(V) from water is a challenging task. In this study, we aim to develop a simple method to produce a highly reactive iron-based reactive media mixture, namely, the activated iron media (AIM), and to evaluate the AIM technology as a potential solution for treating Sb-contaminated water. For the purpose, batch tests were conducted to evaluate the optimum recipe, conditions and procedures to synthesize the AIM and to evaluate the performance of the AIM for removing Sb(V).

Batch tests using serum vial as reactors showed that aeration of $Fe^{2+}$ under alkaline condition could result in formation of mixed Fe(II)-Fe(III) oxide crystalline (FeOx). The composition and structure of resulting FeOx varies greatly with the dosage of $O_2$. With a stoichiometric dosage of $O_2$/Fe(II) at 1:6, magnetite ($Fe_3O_4$) was the product from the oxidative precipitation of $Fe(OH)_2$ by $O_2$, which was corroborated by a ratio of Fe(III)/Fe(II) at 2:1 as well as an inverse-spinel structure identified by X-ray diffraction (XRD) spectroscopy. When zero-valent iron (ZVI) was added into a $Fe(OH)_2$ system, ZVI could consume some of the introduced $O_2$, which resulted in a lower Fe(III)/Fe(II) ratio in the formed FeOx than the one without ZVI. With aeration, ZVI surface was corroded and formed a FeOx coating similar to those FeOx formed from

oxidative precipitation of $Fe(OH)_2$ in term of crystal structure and composition. When the dosage of $O_2$ to $Fe^{2+}$ was doubled to 1:3, the Fe(III)/Fe(II) ratio in the resulting FeOx was near 2.3:1, close to the desired ratio of FeOx in the mixture of the AIM. The batch tests and scaled-up pilot test showed that with appropriate dosage and intensity of $O_2$ aeration, the mixture of ZVI and $Fe^{2+}$ with controlled alkalinity could be converted to form a mixture of highly reactive media with a magnetite-like FeOx in form of a coating on ZVI or discrete crystalline.

Batch tests using the activated iron media to treat Sb-contaminated water was conducted to evaluate effectiveness of the media for Sb removal under various conditions. Under an anaerobic condition, Sb(V) removal consists of rapid removal within the initial 15 min, followed by a slower phase before entering a stagnant phase, which could be better modelled as a chemisorption. Both externally supplied $O_2$ and $Fe^{2+}$ would somewhat help Sb(V) removal by the AIM, but with the co-presence of $O_2$ and $Fe^{2+}$, Sb(V) removal by the AIM could be greatly enhanced, in which a treatment of 50 mg/L with 10 g/L AIM could decrease Sb(V) to below 6 ug/L, the EPA drinking water maximum contaminant level (MCL). Sequential dosing test showed that such high removal of Sb(V) could be sustained in a continuous flow treatment system.

This study has expanded our knowledge of the AIM water treatment system for industrial wastewater treatment, in particular with applications involving extremely high concentration of Sb(V).

# ACKNOWLEDGEMENTS

I would like to express my gratitude to my adviser and committee chair, Dr. Xingmao Ma, and Co-chair Yongheng Huang for offering me the opportunity and guidance in the completion of my master's degree. I am fortunate to get the opportunity to be involved in water quality engineering and gain invaluable experiences performing research in water quality laboratory. I would also like to thank Dr. Chang for serving on my committee.

Additionally, I truly appreciated the company of my fellow colleagues in and out of the laboratory that kept me engaged and evaluated my work along the way. And lastly, thanks for the support of my family from South Korea that permitted me to pursue higher education at Texas A&M University.

# CONTRIBUTORS AND FUNDING SOURCES

## Contributors

This work was supervised by a thesis committee consisting of Professor Xingmao Ma of the Department of Civil Engineering and Professor Yongheng Huang, of the Department of Biological and Agricultural Engineering.

All work for the thesis was completed by the student, under the advisement of Professor Xingmao Ma of the Department of Civil Engineering and Professor Yongheng Huang of the Department of Biological and Agricultural Engineering.

The data analyzed in the discussion for Chapter 4 was provided by Professor Yongheng Huang. These data were collected in part by Dr. Lin Xu of the Department of Biological and Agricultural Engineering.

## Funding Sources

This work was made possible by the fund provided by Evoqua Water Technologies Inc through a sponsored research and development contract signed between Texas A&M University System and Evoqua (formerly, Siemens Water Technology Inc.) as part of a licensing agreement for the commercialization of the hybrid zero-valent iron technology invented by Professor Yongheng Huang at the Department of Biological and Agricultural Engineering.

# NOMENCLATURE

| | |
|---|---|
| AIM | Activated Iron Media |
| As(III) | Arsenite or trivalent arsenic |
| As(V) | Arsenate or pentavalent arsenic |
| $Ca_2Sb_2O_7$ | Roméite |
| Cu(II) | Copper |
| $Fe^{2+}$ | Ferrous iron, or divalent iron |
| $Fe^{3+}$ | Ferric iron, or trivalent iron |
| FeOx | Iron oxides |
| $Fe(OH)_2$ | Iron hydroxide |
| $FeCl_2$ | Ferrous chloride |
| $FeCl_24H_2O$ | Ferrous chloride tetrahydrate |
| α-FeOOH | Goethite |
| β-FeO (OH) | Akaganeite |
| γ-FeOOH | Lepidocrocite |
| $\alpha$-$Fe_2O_3$ | Hematite |
| $\gamma$-$Fe_2O_3$ | Maghemite |
| $Fe_3O_4$ | Magnetite |
| HCl | Hydrochloric Acid |
| $H_3SbO_3$ | Stiborous Acid |
| $HNO_3$ | Nitric Acid |

| | |
|---|---|
| hZVI | Hybrid Zero-Valent Iron |
| ICP-MS | Inductively Coupled Plasma Mass Spectrometry |
| $KSb(OH)_6$ | Potassium hexahydroxoantimonate |
| M | Molarity (moles/L). |
| $Mn^{2+}$ | Divalent Manganese |
| $MnO_2$ | Manganese oxide |
| $Mn(OH)_2$ | Manganese hydroxide |
| Mo(VI) | Molybdate |
| NaOH | Sodium Hydroxide |
| $NH^{4+}$ | Ammonium Ion |
| $NO_3^-$ - N | Nitrate as Nitrogen |
| Sb(III) | Trivalent Antimonial |
| Sb(V) | Pentavalent Antimonial |
| $Sb(OH)_3$ | Antimony Tri-hydrate |
| $Sb(OH)_6^-$ | Antimony Hepta-hydrate |
| $Sb_2S_3$ | Stibnite |
| $Sb_2O_3$ | Valentinite |
| $Sb_2O_5$ | Antimony pentoxide |
| $SbCl_3$ | Antimony tricloride |
| Pb(II) | Lead |
| $Pb_2Sb_2O_7$ | Bindheimite |
| ZVI | Zero-Valent Iron |

TABLE OF CONTENTS

Page

LIST OF FIGURES

Page

LIST OF TABLES

Page

# CHAPTER I

# INTRODUCTION

## 1.1 Problem statement

Antimony(Sb) is an element that belongs to Group XV of the periodic table, along with Arsenic(As). It mainly exists as Sb(III) and Sb(V) in nature (Filella and May, 2003). At thermodynamic equilibrium, in an oxic system, Sb(V) is predominately present as $Sb(OH)_6^-$, but Sb(III) is present mainly as $Sb(OH)_3$ under anaerobic conditions (Filella and May, 2003; Filella and May, 2005). However, a study reported that Sb(V) was detected significantly in the oxygen-depleted system (Filella et al., 2002). The speciation of antimony in an aqueous system is more complicated than the calculation of thermodynamic equilibrium (Filella and May, 2005). Generally, the concentrations of antimony are less than 1 μg/L in unpolluted water (Filella et al., 2002). Antimony has been consumed worldwide in large quantities (> $10^5$ tons/year) in a variety of industries, including additive in ceramics, battery, catalysts, and flame retardants (Leuz et al., 2006). Elevated concentrations of antimony have been reported around mines and in shooting ranges (He, 2007; Scheinost et al., 2006). China produces approximately 90% of the world antimony consumption (Herath et al., 2017). The antimony concentrations in surface water around Xikuangshan in Hunan province reported 1300 to 5000 times above the Chinese drinking water limit (Zhu et al., 2009).

Since antimony is an increasingly identified pollutant to the environment, the United States Environmental Protection Agency (USEPA) and the European Union (EU)

established the permissible Sb concentrations in drinking water as 6 μg/L and 10 μg/L respectively. (USEPA, 1985a; CEC, 1980). The toxicity of antimony directly depends on its oxidation states. The toxicity of Sb(III) was reported to be significantly higher than the effects of Sb(V). Carcinogenic effects of Sb(III) were detected in the lungs of female rats (Groth et al., 1986). Bioaccumulation in fish, amphibians, invertebrate organisms and plants at the polluted environment were reported in 2011 (Fu et al., 2011; Qi et al., 2011). Concentrated antimony was detected from human hair around Xikuangshan antimony mine (Liu et al., 2011). In the environment, $Sb(OH)_3$ adsorbed more than $Sb(OH)_6^-$ due to low solubility and neutral characteristics over wide range of pH levels (Filella et al., 2002; Llgen et al., 2014). $Sb(OH)_6^-$ has weaker binding on the solid surface than that of As(V) because of its large ionic radius and low charge density (Wilson et al., 2010). Thus, Sb(V) could be more mobile in the neutral and alkaline environment and, hence, this study targets removal of dissolved Sb(V) from water.

Multiple technologies have been reported for the remediation of antimony-containing drinking water and wastewater, including electrolytes, membrane separation, coagulation, adsorption, and chemical reduction (Kang et al., 2000; Navarro and Alguacil, 2002; Kang et al., 2003; Saito et al., 2004; Guo et al., 2009; Wu et al., 2010). Among these technologies, adsorption was promising due to the advantage of higher efficiency, low cost, and ease of performance (Li et al., 2015). However, Sb(V) adsorption was sensitive to environmental factors such as pH, ion strength, temperature, etc (Xu et al., 2006; Ettler et al., 2007; Verbinnen et al., 2013). On the other hand, Sb(V)

could be stabilized by incorporating it into the structure of iron oxide, and, hence, the influence of environmental factors was less effective (Mitsunobu et al., 2010).

Zero-valent iron (ZVI) with a standard redox potential of $E_0$ ($Fe^0/Fe^{2+}$) = −0.44V (Shokes et al, 1999), is a versatile and effective reductant that ZVI has been extensively applied for the treatment of wastewater contaminated with various organic and inorganic contaminants (Guan et al., 2015). Due to the advantages of ZVI such as lower cost and ease to apply in large quantities and non-toxicity, ZVI-based techniques has been developed for environmental remediation applications, e.g., reducing heavy metals, and transforming chlorinated organic compounds into less or non-toxic variants of molecules (Fu et al, 2014). Moreover, ZVI could remove contaminants in water via adsorption, co-precipitation, and reduction (Noubactep, 2013). Despite the promising technology to remove the contaminants in wastewater, the passivation of ZVI significantly diminish the reactivity of ZVI. When the surface of ZVI is exposed to the wastewater, the iron oxide layer is formed subsequently due to the iron corrosion. The iron oxide layer is chemically passive and weaken the removal efficiency of target contaminants. Satapanajaru et al. (2003) reported that the maghemite layer may demote the reactivity of ZVI.

To tackle the passivation problem, various methods were studied such as reducing the size and acid washing. Although nano scale zero valent iron media has advantages of rapid remediation, relatively lager reactive area, after the reaction, separating the ZVI particle from the solution is a main issue (O'Carroll et al, 2013). Acid washing is employed to remove the passive later to enhance the reactivity of ZVI

(Agrawal and Tratnyek, 1995). On the other hand, employing acid washing also has several drawbacks: (1) the strong acidic level of wastewater with highly concentrated iron ions; (2) the acceleration of iron corrosion by the $H^+$ ions.

Several studied reported that additives, including activated carbon, $Fe_2O_3$, $Fe_3O_4$ and $MnO_2$ were added (Luo et al., 2014; Shi et al., 2014; Huang at et., 2013; Noubactep et al., 2011) to solve the passivation problem. Moreover, additional aqueous $Fe^{2+}$ promoted the removal efficiency of molybdate by ZVI (Huang et al., 2012). Huang et al. demonstrated that $Fe_3O_4$ and aqueous $Fe^{2+}$ play important role in sustaining the reactivity of ZVI and developed an Actived Iron Media (also called hybrid zero-valent iron) ZVI/$Fe_3O_4$/$Fe^{2+}$ system (Huang et al., 2003; Huang and Zhang, 2006). During the redox reaction between contaminants and ZVI, magnetite could mediate the electron (Xu et al., 2013). Previous studies demonstrated that the active iron media system could effectively remove heavy metals at laboratory and pilot scale tests (Huang et al., 2013; Huang et al., 2013).

The activated iron media consists of three components: (1) zero-valent iron grains with a reactive iron oxide surface coating; (2) discrete iron oxides (FeOx) that resemble magnetite in crystalline structure and composition; and (3) surface-bound Fe(II) that could come from externally added dissolved $Fe^{2+}$. The core feature of the activated iron media is the formation and presence of a sufficient amount of a highly reactive iron oxide species, both on the ZVI surface as a coating and also in discrete form of suspended crystalline. The reactive iron oxides may not have a well-defined

composition and structure, but often feature characteristic of a non-stoichiometric and mixed-valence of Fe(II)/Fe(III) with an inverse-spinel crystalline structure.

To prepare the activated iron media, the old method (Huang et al 2012) is to mix ZVI in a solution with designed amount of nitrate and $Fe^{2+}$, creating a reactive system in which nitrate was reduced by ZVI in the presence of dissolved $Fe^{2+}$ to first form a magnetite coating on ZVI grain surface and over time accrue a significant account of discrete magnetite crystalline in the mixture. This synthesis method is adequate for laboratory use, but may not be desirable for industrial scale application of preparing the activated iron media. The main drawbacks are in three aspects: (1) the process would convert nitrate into ammonium, which is a water contaminant that is regulated and should not be discharged freely; (2) the process is relatively slow; (3) the process is also chemical intensive as it consumes both ZVI and nitrate in order to produce a large amount of FeOx.

In this study, we aims to develop a more cost effective method to prepare the activated iron media. A simpler method worth of trying is to use $O_2$ (air) to oxidize $Fe(OH)_2$ and the surface of ZVI under control chemical conditions to form a highly reactive FeOx phase and surface coating on ZVI grains. The main raw materials to be used will include ferrous salts (e.g., $FeCl_2$), zero-valent iron, and base (e.g., NaOH). As the first step, we aim to synthesize FeOx through oxidation of $Fe^{2+}$ under appropriate pH/alkalinity and $O_2$ dosage conditions. We will evaluate how the structure and composition of FeOx could change with the change of $O_2$ dosage. Once establishing the recipe for FeOx synthesis through oxidative precipitation of $Fe^{2+}$, we will then add ZVI

into the reactive system and evaluate (1) whether the controlled aeration could form a reactive iron oxide coating on the ZVI surface; (2) how the presence of ZVI could alter the chemistry of $Fe(OH)_2$ towards FeOx synthesis; and (3) if we need to alter the recipe and procedure in order to create a high quality activated iron media system.

# CHAPTER II

# LITERATURE REVIEW

## 2.1 Chemistry of antimony

Antimony (Sb) is the element with an atomic number of 51 in the group XV in the periodic table. Like other elements in the group of XV, antimony has allotropic modifications. It is a gray metalloid commonly associated with the stable sulfide mineral Stibnite, which may transform into the mineral Valentinite. Antimony is occasionally found in the explosive and unstable antimony trichloride, however, conversion to the stable forms occurs easily.

Pure antimony cannot be oxidized at room temperature, but it may be oxidized by metal oxides such as $MnO_2$ in the presence of steam at room temperature. Antimony can exist in several oxidation states such as (-III, 0, III, V). However, two oxidation states (III and V) are most predominant in biological and environmental samples. Antimony is often overlooked as a contaminant because of its low solubility and abundance. However, antimony ions (III and V) can be easily hydrolyzed in aqueous solutions, making it difficult to remove them from water.

### 2.1.1 Speciation in environment

Antimony occurs in fresh water from weathering of rocks and runoff of soils. In aquatic environments, antimony is primarily present in the oxidation states of Sb(III) and Sb(V). Many previous studies have demonstrated that Sb(V) is more dominant than Sb(III) in surface water(Filella et al., 2002; Filella and May, 2003; Elleout et al., 2005).

Sb(III) is typically lower than 10% of the total Sb detected in surface water. (Filella et al., 2002).

It is generally agreed that Sb(V) exists mainly in aerobic conditions while Sb(III) exists in anoxic conditions, exceptions have been reported(Filella and May, 2003). For example, significant amount of Sb(III) in aerobic conditions and substantial amount of Sb(V) in anaerobic conditions were documented (Filella et al., 2002). Some Studies contribute the observation to biological activities or/and slow oxidation kinetics. (Quentel and Filella, 2002; Helz et al., 2002; Leuz and Johnson, 2005). Therefore, the speciation of antimony in water is more complicated (Filella and May, 2005). The Sb(III) is in the form of neutral complex $Sb(OH)_3$ at the pH range of 2-11 while $Sb(OH)_6$ , the complex of Sb(V), is negative (Smith and Martell, 1976).

Antimonic acid is a strong acid that is difficult to isolate as a pure phase. Thus, as the pH increases, polymers can be commonly formed in the solution such as $H_n[Sb(OH)_6]_n$ (Gate and Richardson, 1961a). At the pH range from 4 to 9, $Sb(OH)_6^-$, $H_3SbO_3$ are the main species present. Under highly acidic conditions, $SbO_2^+$commonly exist (Filella and May, 2003). Several studies on the equilibrium on Sb(V) hydrolysis in solution (Lefebvre and Maria, 1963; Mesmer and Baes, 1976) demonstrated that $Sb_2O_5$ generates the antimonate anion even when sparingly dissolved in water (Tourky and Wakkad, 1948). Also, hydroxoantimonate salts are difficult to dissolve in water (Blandamer et al., 1974). Fig. 2.1 shows distribution of antimony species as a function of pH, at 25$^o$C and 1 bar according to Tella and Porokovski (2012).

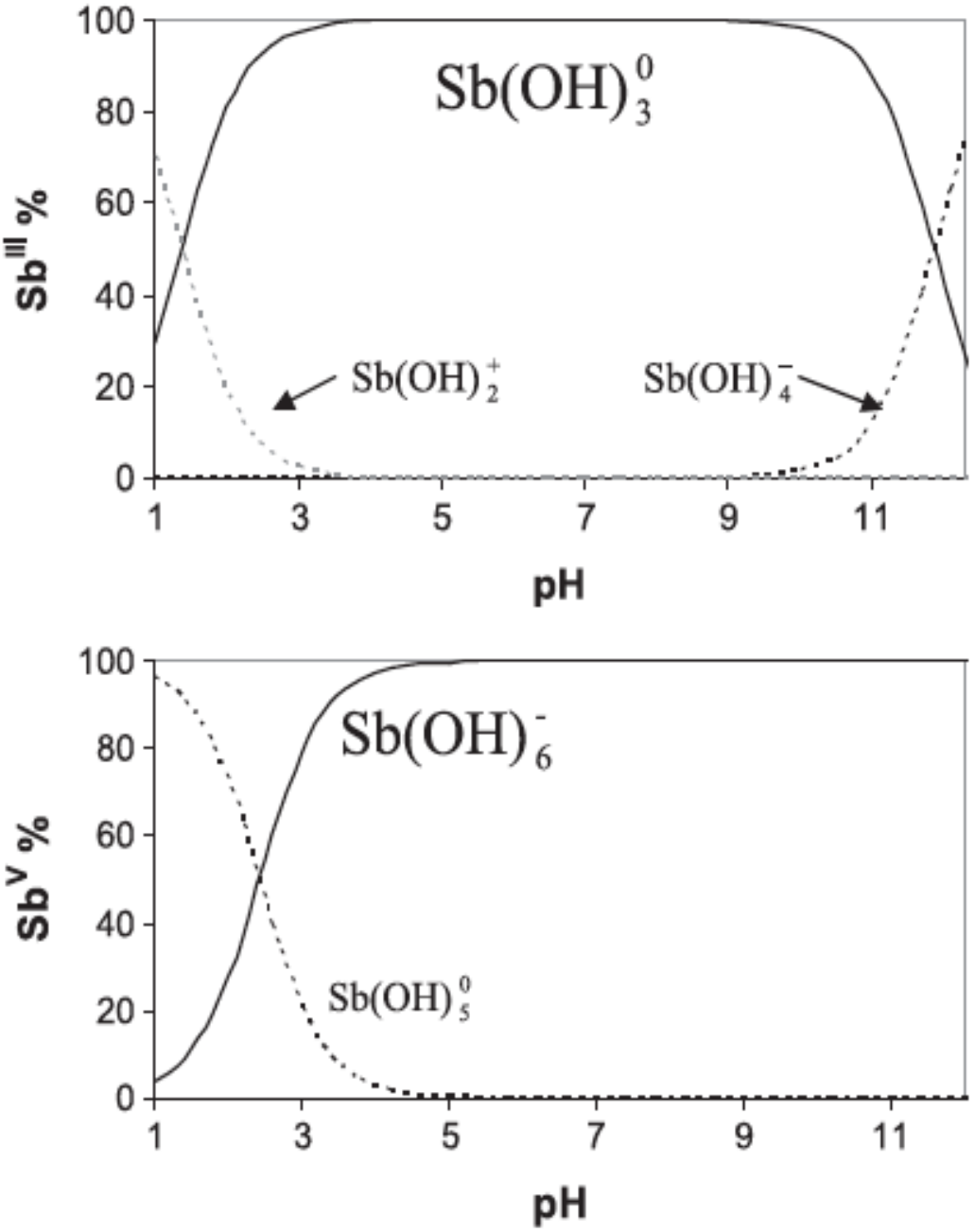


Fig. 2.1 Distribution of antimony species as a function of pH, at 25°C and 1 bar according to Tella and Porokovski (2012).

### 2.1.2 Oxidation

Recently, the oxidation of antimony in aqueous environment has received great attention, particularly related to its removal by iron and manganese hydroxides and oxyhydroxides (Belzile et al., 2001; Leuz et al., 2006a). In 2005 the oxidation kinetics of Sb(III) at 25°C in an aerobic environment were reported (Leuz and Johnson, 2005). The oxidation of Sb(III) was found not to be substantial between the pH range 4-10; however as the pH increased to 11-13, and time required for total Sb(III) oxidation was observed to occur within 4 to 420 days. In this study (Leuz and Johnson, 2005), transformation of Sb(III) species was more favorable when pH was higher than 10, at this higher pH level the transformation of $Sb(OH)_4^-$ to $Sb(OH)_6^-$ (+45.8 kJ/mol) is more likely than the transformation of $Sb(OH)_3$ to $Sb(OH)_6^-$ (+110.6 kJ/mol). The oxidation kinetics of antimony may be improved by hydrolysis. Other cases of oxidation at higher pH include the oxidation of Fe(II) and Mn(II) in aqueous environments. Thus, Leuz and Johnson (2005) observed higher amounts of hydrolyzed antimony species $Sb(OH)_4^-$ when compared with the non–hydrolyzed $Sb(OH)_3$ in their aqueous samples.

In an aqueous environment, trace metals can influence the oxidation of Sb(III). The presence of trace metals such as Cu(II), Mn(II), and Pb(II) will increase the pH, but Zinc(II) has been found to have no effect (Elleouet et al., 2005). Significant acceleration of Sb(III) oxidation by Cu(II) was observed while Mn(II) and Pb(II) were found to have less effect lower acceleration (Elleouet et al., 2005).

A study by Leuz et al. (2006a) reported that the influence of Fe(II) and Fe(III) assisted with Sb(III) oxidation with the various pH range. At pH 2.2 and 3.2 Fe(III) co-

oxidation of Sb(III) was effective, however Fe(II) co-oxidation of Sb(III) was effective at pH ranged above 5. The oxidation kinetics were reported at the same study. At the pH range of 2-3, the Fe(III) oxidized Sb(III) with a pseudo–first order rate and an oxidation time of approximately 1 to 1.5 years, 1 μM Sb(III), 90 μM Fe, at room temperature. As the pH increased to 5-6, the concentration of total antimony was decreased without Sb(III) conversion to Sb(V). One possible reason that this conversion did not occur is probably because of the sorption of Sb(III) onto iron hydroxide colloids. The complete oxidation of antimony (1 μM) was observed within 7 days at pH 5 and 10 hours at pH 6. Therefore, the Fe(III) oxidation was not substantial at pH greater than 5. The total oxidation with Fe(II) was complete in 10 mins at pH 7.

The experiment of the influence of oxygen on the oxidation of 1 μM Sb(III), 90 μM Fe(II) at pH 2-7.6 was also performed. The results demonstrated that the oxidation of Fe(II) in aerobic condition depended significantly on the solution pH. At pH 2-3.6, the oxidation was relatively slow, however, the oxidation accelerated when the pH was neutral. The effect of the ratio of Fe(II) to Sb(III) on the oxidation kinetics of Sb(III) in the pH range of 6.4-7.5 was also investigated. The results suggested that the oxidation kinetics can be enhanced with higher ratio of Fe(II) to Sb(III) and higher pH range (Leuz et al., 2006a).

### 2.1.3 Solubility

Antimony can be accumulated in an aquatic environment due to the weathering of rocks, soil runoff or human activities. Generally, in an unpolluted water, the concentration of dissolved antimony is less than 1 mg/L. However, the concentration can

increase more than 100 times in an environment polluted by anthropogenic sources. The concentration of Ab in an environment is dependent on the solubility of solid phase of antimony. Several Eh-pH diagrams for antimony have been reported (Fig. 2.2) to explain the relationships of phase and solubility in different oxidation states and species, including both aqueous and hydrolyzed Sb. On the other hand, uncertain thermochemical parameters cause previous diagrams to be inaccurate. Moreover, the mobility of Sb(V) under aerobic conditions is not accurately reported due to the metastable phases of antimony included in the calculations. Also, the concentration of cations in samples may lead to the separation of the secondary form of unknown minerals.

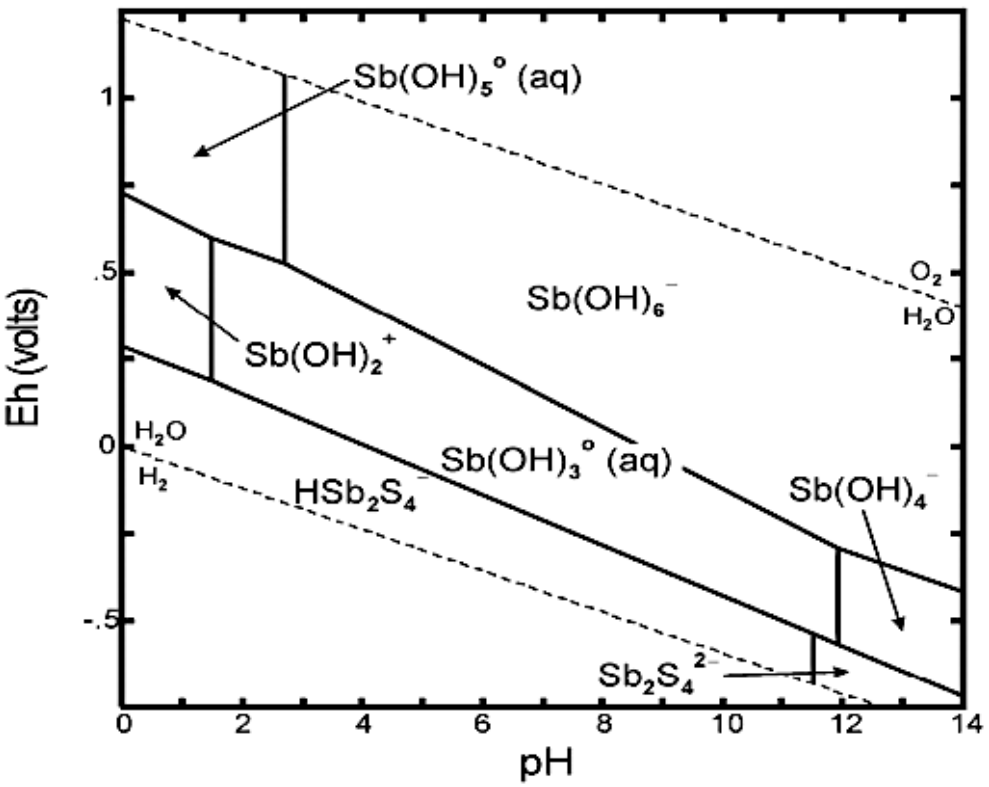


Fig. 2.2 Eh – pH diagram of antimony in the Sb – S –H2O system at 25°C and $10^{-14.6}$ mol/L according to Krupka and Serne (2002).

Previous studies have reported the low solubility of antimony trioxide (Gayer and Garrett, 1952; Filella et al., 2002). Antimony trioxide can be slightly soluble in acid (3 x $10^{-5}$mol per kg water at 25°C) and more soluble in alkali (5 x $10^{-4}$mol per kg 0.1 M NaOH) conditions. In general, between the pH range of 2-10, the solubility of antimony trioxide is not dependent on pH, indicating that undissociated antimony hydroxide can be formed. The formation of antimony hydroxide is shown in equation 2.1.

$$Sb_2O_3 + 3H_2O \leftrightarrow 2Sb(OH)_3 \qquad \text{eq. 2.1}$$

The lack of proper solubility data regarding Sb(V) is limiting the understanding of the behavior of Sb(V) in aqueous environments. The solubility of the mineralized form of Sb(V) was reported between 25-55°C in scientific papers written by Blandamer, Diemar and others (Blandamer et al., 1974; Diemar et al., 2009). At 298.15K, the $K_{sp}$ value of mopungite, brandholzite and bottinoite was $8.89 \times 10^{-6}$, $1.82 \pm 0.15 \times 10^{-8}$ and $1.29 \pm 0.13 \times 10^{-10}$, respectively. Thus, the solubility of these minerals follow the order: mopungite > brandholzite > bottinoite, with the potassium salt as the most soluble. Other studies reported the solubility of $Ca[Sb(OH)_6]_2(s)$ and $Pb[Sb(OH)_6]_2(s)$ at 25°C (Johnson et al., 2005) with a Kso value of $10^{-12.55}$and $10^{-11.02}$ respectively. These amorphous materials are likely crystalized to roméite ($Ca_2Sb_2O_7$), and bindheimite ($Pb_2Sb_2O_7$) under the highly concentrated cations such as Ca or Pb in soil waters (Johnson et al., 2005). These data represents the estimated upper limits of the solubility of Sb(V) in the presence of $Ca^{2+}$(aq) and $Pb^{2+}$(aq) within relatively short reaction times.

## 2.2 Removal methods

Antimony has critical impacts on the environment due to its mobility and complexation reactions in nature. Therefore, international regulations have given priority to the removal of antimony compounds in wastewater. Because of the wide industrial applications of antimony, a significant amount has been released into global aquatic environments. In the past, the surface water and groundwater were crucially polluted by antimony because of the less efficient and the complexity of wastewater treatment. Thus, effective treatment methods of antimony are necessary in order to protect environment and human health.

Presently, the removal technology of antimony is focused on the properties of antimony. Consequently, various chemical and physical treatment methods were developed to control antimony in aquatic environments. Treatment methods evaluated include adsorption, coagulation and co-precipitation and membrane filtration. Among these methods, adsorption is widely applied. There are various factors such as pH, contact time, temperature and specific surface area of the adsorbent that affect the performance of adsorption.

### 2.2.1 Adsorption

The adsorption capacity of various iron based adsorbents for antimony ranged from 0.6 mg/g to 450.4 mg/g. The highest adsorption capacity was 450.4mg/g with akaganeite which has a large specific surface area and high porosity (Kolbe et al., 2011). The Fe-Mn binary oxide was shown to have a high value of 214mg/g (Xu et al., 2011). Importantly, the performance of adsorbents depends on experimental factors such as pH

temperature and contact time (Guo et al., 2014; Miao et al., 2014). However, studies that compare the value of adsorption performance with the same adsorbent and different experimental factors are limited.

One of the influencing factors on the adsorption is pH. There are several studies on the adsorption of antimony within the pH range 2-10 with iron adsorbents (Verbinnen et al., 2013; Guo et al., 2014; Shan et al., 2014). The adsorption rate of iron adsorbents was enhanced when the pH increased from 2-3. However, at the pH range of 3-5 the data shows a plateau, and the adsorption decreased substantially when the pH was increased above 5. A study performed by Verbinnen et al. (2013) reported that the optimum pH range was 3-4 for the enhanced adsorption of Sb(V) with magnetite. Other adsorbents such as hematite and hydrous ferric oxide were reported with similar results (Guo et al., 2014; Shan et al., 2014).

A study conducted by Giasuddin et al. (2007) reported that the pH at the point of zero charge of nZVI was 7.8. The surface of adsorbents is positively charged when the pH range is lower than that of the point of zero charge pH. At this point protonation encourages the removal of antimony. However, when the pH range is higher than that of the point of zero charge pH, the surface of the adsorbent is negatively charged. The Sb(V) exists as an anion in the solution which lead the competition between hydroxyl ions and antimony at the pH range 5 - 10. Therefore, the adsorption of antimony depends on electrostatic repulsion (Deng et al., 2017).

Generally, the value of total adsorption rate can be promoted as the temperature increases (Xu et al., 2006; Miao et al., 2014). The proper temperature for adsorption was

between 15-35°C, and adsorption rate of Sb(III) influenced by the temperature is less than the adsorption of Sb(V) on the ferric adsorbents. Another influencing factor for adsorption rate is the specific surface area. The adsorption of five different crystalized iron oxides was reported in a 2014 study at a pH of 4. In this study, the adsorption rate was increased in the order of HFO > γ-FeOOH > β-FeOOH > α-FeOOH > α-$Fe_2O_3$(Guo et al., 2014). A study conducted by Dai et al. (2014) reported that nanoscale zero valent iron is a practical adsorbent with an increased specific surface area. The results indicated that the number of adsorption sites can be increased as the particle size become smaller. Contrarily, because the particle is small in size, filtration may be difficult. Therefore, both the size and specific surface area of the absorbent need to be considered.

2.2.2 Membrane separation

Membrane separation can be categorized by examining the pore size of a given membrane. Microfiltration (MF), ultrafiltration (UF), nanofiltration (NF) and reverse osmosis (RO) are examples of membranes. The studies on membrane separation for antimony are limited. A study by Kang et al.(2000) reported that the removal of two species of antimony at pH range 3-10 and found that the removal of Sb(V) was higher than Sb(III). However, using RO membrane for antimony removal was not strongly affected by a change of pH range due to rapid antimony oxidation in the sample. In the same study, the arsenic(V) was highly pH dependent when RO membrane removal was applied. Other studies of high removal efficiency of antimony was found when the chelating porous hollow fiber membrane was applied (Nishiyama et al., 2003). However,

limitations of the membrane separation process are the necessity for higher energy consumption and pretreatment for the operation.

### 2.2.3 Coagulation

Coagulation, flocculation, and sedimentation (CFS), are combined treatment technologies employed for heavy metal removal from drinking water. Although alum and iron salts are commonly applied for Sb removal, iron coagulation can remove Sb more effectively (Kang et al., 2003). In 2009, a study reported that 98% of Sb(V) was removed at pH 6 by ferric coagulants, also Sb(III) was shown to be effectively removed at a higher percentage than Sb(V) in the pH range 4-10 (Guo et al., 2009). The order of removal efficiency was As(V) > Sb(III) > As(III) > Sb(V), unlike the arsenic coagulation, the coagulation of Sb(III) has a higher removal efficiency than the Sb(V). The coexistence of humic acids and phosphate in the sample did not interfere with the coagulation of Sb(III), but the Sb(V) removal was substantially affected by the presence of humic acids, phosphate, bicarbonate and sulfate (Wu et al., 2010).

### 2.2.4 ZVI application

ZVI is an elemental iron with zero valent electrons. The ZVI has been applied as a reducing agent for the treatment of contamination in wastewater and groundwater because of its strong potential to abate heavy metals. In 1994, ZVI was applied for degradation of halogenated hydrocarbons (Gillham and O'Hannesin, 1994). Additional investigations have reported that ZVI effectively remove heavy metals such as arsenic, copper, lead, mercury and selenium. The ZVI has a significant potential as a medium because of its low cost and the potential for reuse (Boller and Steiner, 2002). During the

treatment of heavy metals, ZVI can be used for three dominant processes: adsorption, cementation and reduction (Choe et al., 2000; Shokes and Moller, 1999; Smith, 1996).

However, during heavy metal removal, the ZVI is oxidized to Fe(II) and Fe(III) with the reduction of the contaminants (Blowes et al., 1997; Furukawa et al., 2002). Once the iron oxides and oxy-hydroxides such as α-FeO(OH) or $Fe_2O_3$ are formed on the surface of ZVI, the ZVI will lose the potential as a reducing agent due to passivation. On the other hand, the reactivity of ZVI can be promoted with the formation of magnetite or green rusts on the surface of the ZVI (Huang et al., 2003; Mishra and Farrell, 2005).

To tackle the issue of passivation, Huang at et (2013) developed an effective method of keeping the reactivity of ZVI with contaminants in wastewater until the media is exhausted. The method is regulating the aqueous $Fe^{2+}$ to generate a chemical environment to promote the iron corrosion as magnetite at the surface of ZVI. Therefore, the coated magnetite of the outer layer can be discrete with the ZVI grains composing the inner layer. The process is called hybridized ZVI system and is applied as a commercial process for continuous and effective heavy metal treatment such as the PironoxTM by Evoqua Water Technologies LLC (Alpharetta, GA).

The aqueous $Fe^{2+}$ in the hZVI has been reported to play a key role in overcoming the passivation of ZVI (Huang et al., 2003; Zhang and Huang, 2006). On the surface of ZVI, the aqueous $Fe^{2+}$ will form two layers : an inner layer made of magnetite and an outer layer composed of lepidocrocite. In 2003, Huang et al. reported that the ratio of $Fe^{2+}$: $Fe^{3+}$ in the magnetite was 1 : 2. Equation 2.2 is based on the electron balance and mass balance of the formation of magnetite with nitrate as an oxygen source.

$$NO^{3-} + 2.82Fe^{0} + 0.75Fe^{2+} + 2.25H_2O \rightarrow NH^{4+} + 1.19Fe3O4 + 0.50OH^{-} \quad \text{eq. 2.2}$$

Another important factor in the hZVI system is the dissolved oxygen (DO) used to form the iron oxides on the surface of ZVI. On the outer layer of ZVI, lepidocrocite is formed as an iron corrosion product. When the DO is exhausted, the lepidocrocite will return to a magnetite (Tamaura et al., 1983). Therefore, the final formation of iron oxide is magnetite, which has a specific electron conductivity unlike the other iron oxides such as goethite and hematite. The formation of magnetite from the lepidocrocite is shown in equation 2.3.

$$[\gamma\text{-FeO(OH)}]_2\text{FeOH}^{+} \rightarrow \text{Fe}_3\text{O}_4 + \text{H}_2\text{O} + \text{H}^{+} \quad \text{eq. 2.3}$$

There are several studies that have demonstrated the efficient heavy metal removal by the hZVI system. In 2003, Huang et al. conducted a pilot scale demonstration for treating flue gas desulfurization wastewater. In this study, spiked heavy metals (Hg, Se, As, Cd, Cr, Cu and Pb) were reduced from 1 mg/L to near or below 1 μg/L level at a neutral pH by using a multi-structured treatment process. Generally, 99.99% of Hg was removed at all reactors stages. However, the reactor with well crystallized magnetite performed better for selenium removal than the other reactors with altered iron oxide forms such as ferric (oxyhydr)oxides. In 2016, Tang et al. (2016) used a commercial magnetite to from an hZVI system. During the preconditioning, ZVI surface was covered with the magnetite. In this study, selenate was removed 0.253 mM

within 1.5 h as the dissolved $Fe^{2+}$ decreased. Once dissolved $Fe^{2+}$ was exhausted, the removal efficiency was decreased by 20%, but externally supplied aqueous $Fe^{2+}$ allows rejuvenation of the reactivity of an hZVI system to similar levels reported by Huang and Zhang (2005). On the other hand, due to the ammonium from the preparation and relatively slow process, a more cost effective method is needed.

# CHAPTER III

# MATERIALS AND METHODS

## 3.1 Chemicals

Dissolved $Fe^{2+}$ stock solution (0.05 M) was prepared using $FeCl_2 4H_2O$ (≥99%, J.T. Baker), which was augmented with 0.001 M HCl in order to hinder the oxidation of $Fe^{2+}$ in the solution. Sb(V) stock solution (1000 mg/L) was prepared using $KSb(OH)_6$ (≥99%, Honeywell). NaOH stock solution (0.05 M) was prepared using NaOH pellets (≥98%, VWR international). To dissolve the reagents, deoxygenated deionized (DDI) water with a resistivity of >15 MΩ (E-pure D4641, USA) was used. Dissolved oxygen (DO) in Deionized (DI) water was eliminated by bubbling nitrogen gas at a flow rate of ~10 L/min for 40 mins in a 4 L container. All solutions were prepared in an anaerobic chamber containing approximately 95% $N_2$/ 5% $H_2$ with a palladium catalytic oxygen gas removal system (Coy Laboratory, USA). HCl (6N, J.T. Baker) was used to adjust pH of the reagent solution. ZVI (iron power 100-mesh ≥98%, Macron Fine Chemicals) was applied for all tests.

## 3.2. Analytical Methods

### 3.2.1 Wet chemistry

Water quality analyses: pH, $Fe^{2+}$, $Fe^{3+}$, total Fe, Sb(III), Sb(V) pH measurements were conducted using Orion 5 Star pH meter (Thermo Fisher Scientific, Singapore). Dissolved $Fe^{2+}$ and total Fe were measured colorimetrically by a UV-VIS spectrometer (T80, PG Instruments) using the 1,10-phenanthroline method, which reported a minimum detection limit of 0.1 mg/L. For total Fe analysis, the sample was pretreated

with Hydroxylamine hydrochloride to reduce $Fe^{3+}$ to $Fe^{2+}$ as the first step before analysis. Dissolved $Fe^{3+}$ was determined by subtracting dissolved $Fe^{2+}$ from total Fe concentration. Sb was analyzed using ICP-MS (Agilent 7700).

3.2.2 Material characterization: ratio of Fe(III)/Fe(II) in FeOx, XRD

To determine the crystal structure of generated iron oxide, the solids retained on the filter paper was rinsed with DDI, and the solids together with the membrane were stored in the anaerobic chamber and kept dry until the XRD analysis was conducted. The X-ray power diffraction were conducted by using XRD (Bruker D8 powder X-ray diffractometer) equipped with a monochromatized Cu K$\alpha$ radiation.

### 3.3 Preparation of the Activated Iron Media

One task of this study is to develop a novel method to prepare the activated iron media. The effort consists of three phase. In the first phase, we use serum vial as the reactor to synthesis iron oxide(s) in batch mode through controlled oxidation of ferrous hydroxide by $O_2$. In the second phase, also with serum vial, ZVI was added to the mixture and evaluate if ZVI/$Fe(OH)_2$ system could be converted into an activated iron media system with $O_2$ aeration under controlled conditions. In the third phase, a 200 L reactor tank was employed to demonstrate that the recipe and knowhow developed from the serum vial batch test could be employed to create the activated iron in large scale.

3.3.1 Formation of FeOx through oxidation of $Fe^{2+}$ by $O_2$

As the first step to develop the AIM (ZVI/$Fe_3O_4$), we use serum vial as batch reactor to evaluate FeOx formed from the oxidation of $Fe(OH)_2$ by $O_2$. For this test, 70 mL serum bottles were used as reactors. The reactants were prepared in an anaerobic chamber as shown in Figure 3.1. In the reactor, 0.6 mL of $Fe^{2+}$ stock solution (0.05 M), 1.28 mL of NaOH (0.05 M) and 38.12 mL of DDI water were filled to make a total reactant mixture of 40 mL. The mixture initially contained 0.75 mM $Fe^{2+}$ and 1.6 mM NaOH. $Fe^{2+}$ would react with NaOH to from $Fe(OH)_2$ precipitate immediately after mixing. With NaOH slightly overdosed, the initial pH was in the alkaline condition. The reactors were sealed immediately with a rubber stopper.

Fig. 3.1 Photograph of the anaerobic chamber used in this study

With 40 mL reactant solution in 70 mL serum bottle, the reactor had 30 mL of headspace that was made up of 95% $N_2$ and 5% $H_2$ from the anaerobic chamber. To equilibrate the headspace pressure with the atmosphere, two needles were poked through

the rubber stopper. A specific amount of volume of gas (0 mL, 0.278 mL, 0.555 mL, 1.21 mL, and 2.42 mL) from the headspace was extracted by first syringe and replaced with air by the second syringe, so that different amount of $O_2$ was spiked in the headspace. The introduced air from the second syringe was the only $O_2$source for this test. After the reactors were sealed with an aluminum crimp on the rubber stopper, the reactors were completely mixed for 20 hours in a rotating tumbler at 30 rpm in the dark at room temperature.

After mixing for 20 hours, the reactors were returned to the anaerobic chamber. 15 mL liquid mixture (with iron oxide suspension) was withdrawn from each reactor with a syringe. The extracted solution was separated into a 5 mL and a 10 mL sample. To quantify Fe(III)/Fe(II) in the formed FeOx precipitate, 5 mL of 6N HCl was added into the 5 mL suspension sample. After the solids were dissolved completely, the solution was diluted 5-10 times with DDI and analyzed for dissolved $Fe^{2+}$ and $Fe^{3+}$ to determine the ratio of Fe(III)/Fe(II) in the formed FeOx. To verify the Fe(II)/Fe(III) molar ratio of synthesized magnetite, commercial magnetite (Alpha chemicals, USA) sample with a known ratio of Fe(II)/Fe(III)=1:2 was used to conduct a quality control test with the same procedure.

The 10 mL suspension sample was filtrated through 0.45 μm membrane disc filter (Pall Gelman). The filtrate was analyzed for dissolved $Fe^{2+}$ and $Fe^{3+}$. pH was measured immediately.

To determine the mass of precipitated solids, parallel experiments were repeated. The reactors which was introduced 0.555 mL of air at the headspace were

transferred into the anaerobic chamber from the rotating tumbler after 20 hours. In the anaerobic chamber, precipitated solids were rinsed with DDI twice. A strong magnet was placed at the bottom of the reactors to hold the produced suspended solids. After the reactor was removed from the anaerobic chamber, the solution was filtered with a 0.45 μm membrane filter to separate the suspended solids from the solution. The mass of suspended solid was calculated by subtracting the mass of the membrane filter from the total mass.

To determine the crystal structure of generated iron oxide, the solids retained on the filter paper was rinsed with DDI, and the solids together with the membrane were stored in the anaerobic chamber and kept dry until the XRD analysis was conducted.

### 3.3.2 Preparation of the Activated Iron Media in serum bottle

Preparation of the Activated Iron Media using $O_2$ as the oxidant was also first evaluated using 70 mL serum bottles through batch tests. 10 mg of 100-mesh ZVI powder (Macron Fine Chemicals) was added into the serum bottles, followed by adding designed amounts of $Fe^{2+}$ and NaOH stock solution as well as DDI water to make 40 mL reactant mixture with 0.75 mM $Fe^{2+}$ and 1.6 mM NaOH. No additional pH adjustment was conducted. The reactors were sealed tightly with rubber stoppers. A certain volume (0 mL, 0.278 mL, 0.555 mL, 1.21 mL, and 2.42 mL) of air was injected into the headspace by a needle through the rubber stopper. The same volume of gas was withdrawn before the injection of air to equilibrate the atmospheric pressure. On the rubber stopper, an aluminum crimp was used to seal the reactors tightly. Then, the

reactors were placed in a rotating tumbler and completely mixed for 20 hours at 30 rpm at room temperature.

After the 20 h mixing, the reactors were withdrew from the tumbler and placed in the ultrasonic cleaner (1.9 L, 150W, VWR Scientific) for the sonication. All the reactors were placed at the center of the ultrasonic cleaner to assure the same sonication condition. The iron corrosion product in form of an iron oxide coating on ZVI grain surface was started to be stripped off from the surface of ZVI by sonication. After sonicating for 0.5 min, all the reactors were transferred to the anaerobic chamber. Afterwards, the ZVI powder (100-mesh) was allowed to settle down in the reactors. 10 mL liquid mixture with suspended precipitate was withdrawn from the reactors with a syringe.

The withdrawn solution was separated into two 5 mL samples to measure the pH and ratio of Fe(II)/Fe(III). Each 5mL solutions were placed in a 10 mL serum vials. To dissolve the suspended solids, 5 mL 6N HCl was injected in a 10 mL serum vial in order to determine the total iron. To analyze the molar ratio Fe(II)/Fe(III), the solution was diluted 5-10 times with DDI after the iron oxides were completely dissolved.

3.3.3 Pilot scale production of the activated iron media

To demonstrate the feasibility of the new media preparation method, 200L reactor was used as a scaled up test. The reactor was filled with 200 L tap water; 2.88 kg $FeSO_4.7H_2O$ salt was added into the reactor. The mixer was turned on to dissolve $FeSO_4$ salt. 0.822 kg of NaOH was then added into the reactor, which dissolved quickly and reacted with $Fe^{2+}$ to form $Fe(OH)_2$ precipitate. NaOH was slightly overdosed, which was

to ensure the reactant mixture has an initial alkaline condition with a pH of about 11. 2 kg of ZVI (5 um size) was then added. The aeration pump was then turned on and the flow rate was regulated through a needle valve to provide a designed air flow rate of 11 L/min.

**3.4 Antimony removal tests**

The antimony removal test was conducted in 10 mL vials with 10 g/L, 20 g/L, 30 g/L, 40 g/L, and 50 g/L of produced AIM from Preparation of the Activated Iron Media in 70 mL bottle. All the reactors were transferred into the anaerobic chamber. In the anaerobic chamber, a strong magnet was placed at the bottom of the reactors to hold the produced suspension. The suspended solids were rinsed with the DDI water twice and 50 mg/L of Sb(V) stock solution was injected into the reactors. All the reactors were sealed immediately with a rubber stopper and an aluminum crimp. Then, the reactors were transferred in a rotating tumbler for mixing at 30 rpm and room temperature. At the 5 min, 15 min, 30 min, 1 h, 1.5 h, 2 h, 3 h, 4 h, 6 h, 9 h and 10 h, the reactors were withdrawn and 10 mL of solution was extracted by the syringe. Immediately, the pH measurement was conducted by using the 5 mL solution. Another 5 mL solution was filtered with a 0.45 μm filter and placed in 10 mL serum vials to measure the aqueous Fe(II) and Sb(V). Sb(V) measurement was conducted by an Inductively Coupled Plasma Mass Spectrometry (ICP-MS, 7700, Agilent Technology, USA). The solution samples were diluted by 5–10 times with 2% of the $HNO_3$ solution if dilution is needed.

3.4.1 Control test

To evaluate the ratio of AIM and Sb removal, five different level of AIM were

introduced with 50 mg/L of Sb(V). AIM only or AIM/Fe(II) system were tested for the Sb removal. The tests were conducted at room temperature. Samples were extracted from reactors at 5 min, 15 min, 30 min, 1 h, 1.5 h, 2 h, 3 h, 4 h, 6 h, 9 h and 10 h. The pH and Sb(V) in supernatant were measured immediately same as above.

3.4.2 Aerobic and Anaerobic condition tests

To evaluate the benefit of $O_2$ and Fe(II) on Sb removal, four different systems are applied. The concentration of Sb(V) was 50 mg/L and the AIM was 10 mg/L for all Group. Group 1 was applied AIM without additional Fe(II) solution and $O_2$. Group 2 was applied AIM with 0.5mM of Fe(II) stock solution. Group 3 was applied AIM with spiked $O_2$ gas 1 mL/h. Group 4 was applied AIM with both of 0.5mM of Fe(II) stock solution and 1 mL/h of pure $O_2$ gas. The tests were conducted for specific time (5 min, 15 min, 30 min, 1 h, 1.5 h, 2 h, 3 h, 4 h, 6 h, 8 h and 10 h) at 30 rpm dark rotating tumbler at room temperature. The pH and Sb(V) in supernatant were measured immediately same process as above.

3.4.3 pH test

The purpose of this test was to examine the dependence of antimony removal on different pH levels. In this study, the pH was controlled with the level of 3, 5, 7, 9, and 11 respectively. The initial concentration of Sb(V) was 50 mg/L and the AIM was 10 mg/L. The reactors were mixed for 4 hours in the rotating tumbler at room temperature and 30 rpm. The pH and Sb(V) in supernatant were measured immediately same methods as above.

3.4.4 Sequential dosing test

Sequential dosing tests were conducted to elucidate the role of Fe(II) in the AIM/Fe(II) system. Multiple tests were conducted at the 70 mL serum reactors were with an initial 50 mg/L antimony(V), and ZVI or AIM were 50 mg/L. The reaction was conducted at 30 rpm dark rotating tumbler at room temperature. At designed time (15 min, 30 min, 1 h, 1.5 h, 2 h, 3 h, and 4 h), 2 mL solution was extracted and by the syringe and filtered through 0.45 μm filter to monitor dissolved antimony(V) and ferrous. At designed time intervals, another dosage of 50 mg/L antimony and 0.3 mM, 0.5 mM, and 0.8 mM of Fe(II) were added. The pH and Sb(V) in solution were measured immediately same as above.

**3.5 Statistical data analysis**

Data were subjected to two-way analysis of variance analysis (ANOVA) and one-way analysis of variance analysis (ANOVA). Experimental design was randomized with two different factors (aqueous $Fe^{2+}$, $O_2$). Mean comparison was obtained by Tukey Kramar HSD (honestly significant difference) test. The removal efficiency data of Sb(V) were analyzed by JMP Pro 13 (SAS Institute Inc., NC).

# CHAPTER IV

# RESULT AND DISCUSSION

## 4.1. Preparation of the Activated Iron Media

### 4.1.1 Effect of $O_2$ dosage on the Fe(II)/Fe(III) ratio of FeOx

The test was conducted to form magnetite from aqueous $Fe^{2+}$ through an aeration process. Synthesis of FeOx was conducted with varying amount of $O_2$ to evaluate the impact of $O_2$ dosage on the formation and composition of FeOx.

In this section, we aim to evaluate (1) if stoichiometric dosage of $O_2$ would form a FeOx phases as magnetite; (2) how the aerated $O_2$ could affect the crystal structure of FeOx.

As described in Chapter 2, a series of batch tests were conducted with initial concentrations of 0.75 mM $Fe^{2+}$ and 1.55 mM NaOH. Various amounts of $O_2$ were introduced into the reactor headspace by the syringe to oxidize $Fe(OH)_2$ to form $FeO_X$. A

study by Kiyama (1974) reported that magnetite can be synthesized in a water through oxidation of $Fe(OH)_2$. Equation 4.1 illustrates the stoichiometric amount of $O_2$ to generate magnetite.

$$3\ Fe^{2+} + 6\ OH^- + 0.5\ O_2 = Fe^{(III)}{}_2O_3Fe^{(II)}O + 3\ H_2O \qquad \text{Eq. 4.1}$$

For the amount of $Fe^{2+}$ (0.75 mM in 0.04 L), it would consume 0.005 m mol $O_2$, which could be provided by 0.56 mL air at 22 C and 1 atm. After 20 h reaction, iron oxide precipitate formed in the reactor were sampled and analyzed to determine the Fe(III)/Fe(II) ratio and crystal structure.

Immediately after the addition of NaOH, $Fe^{2+}$ would react with $OH^-$ to form $Fe(OH)_2$, a white precipitate. Once $O_2$ was introduced into the reactor headspace and mixed with the reactant, $Fe(OH)_2$ precipitate would be quickly oxidized to become a greenish precipitate and then further evolve depending on $O_2$ dosage. After 20 h reaction, the reactions were consider completed. FeOx in form of precipitate was observed in all reactors. At the end of reaction, the pH of the all reactor mixture was near 9.3, a weak alkaline condition. In the tests with $O_2$ dosage close to the stoichiometric amounts, FeOx was found to be in form of black precipitate in the tests with relative $O_2$ dosages of 1 and 2 in Figure 4.1 In the tests with relative $O_2$ dosages of 0.5 and 4 (Figure 4.1), FeOx was found to be in form of brownish precipitate. Magnetite was black while maghemite has a color of dark brownish.

The results of the chemical analysis of Fe(III) : Fe(II) ratio of the precipitated FeOx are shown in Figure 4.1. As the $O_2$ dosage increases, the ratio of Fe(III) : Fe(II) increased from 0.2 to 4.4. At Fe(III)/Fe(II)=4.4, the formula of FeOx could be

represented as $Fe(III)_{4.4}Fe(II)O_{7.6}$, which could be seen as a mixture of $Fe_3O_4$ and $Fe_2O_3$. In the test with a stoichiometric dosage of $O_2$ (0.56 mL air), the ratio of Fe(III) : Fe(II) were close to 2, which conforms reaction Eq.4.1. The result suggests that the precipitated solid was $Fe_3O_4$ (magnetite). A study reported the Fe(III) : Fe(II) ratio of $Fe_3O_4$ (magnetite) as 2 with inverse spinel structure (Dang et al., 2007). A key finding from these tests is that the composition of FeOx, more specifically, the Fe(III)/Fe(II) ratio, depends greatly on the dosage of $O_2$. Equation 4.1 only represents a special case of the oxidation of $Fe(OH)_2$ by $O_2$.

In order to verify the precipitated FeOx with the stoichiometric dosage of $O_2$ as $Fe_3O_4$ (magnetite) the net mass was measured after the 20h reaction. The difference between measured mass of generated magnetite (21.6 mg) and the theoretical value (23.15 mg) was less than the 10%. The collected FeOx sample were analyzed using XRD. No other peaks were found from XRD spectrum (Fig. 4.2) except the peaks of magnetite (or maghemite). Magnetite and maghemite ($\gamma$-$Fe_2O_3$) share almost identical XRD pattern as the two have a very similar structure—an inverse spinel structure that the difference of the two spectra was not obvious in XRD spectrum. Even the dosage of $O_2$ was increased twice, the XRD spectrum of precipitated FeOx showed no difference with the Figure 4.2. The result suggested that magnetite could be further oxidized over time toward becoming maghemite when $O_2$ is in excess, but the overall crystalline structure would remain the same despite the increased fraction of Fe(III) to Fe(II).

Oxidation of $Fe^{2+}$ through aeration under alkaline condition could produce FeOx precipitate. The composition of FeOx depends on the dosage of $O_2$. When a

stoichiometric dosage of $O_2$ is supplied, magnetite with an ideal ratio of Fe(III)/Fe(II) =2 could be produced. Additional $O_2$ supply could further oxidize $Fe_3O_4$ towards $Fe_2O_3$. While the Fe(III)/Fe(II) ratio increased significantly with elevated dosage of $O_2$, the basic crystal structure of $FeO_x$ will remain largely unchanged in form of an inverse spinel structure that is a characteristics of magnetite.

The above test results suggested that aeration of $Fe^{2+}$ under carefully controlled conditions such as appropriate pH, alkalinity, and intensity and duration of aeration, might be a viable method to synthesize desired FeOx product that is a key component of the active iron media system.

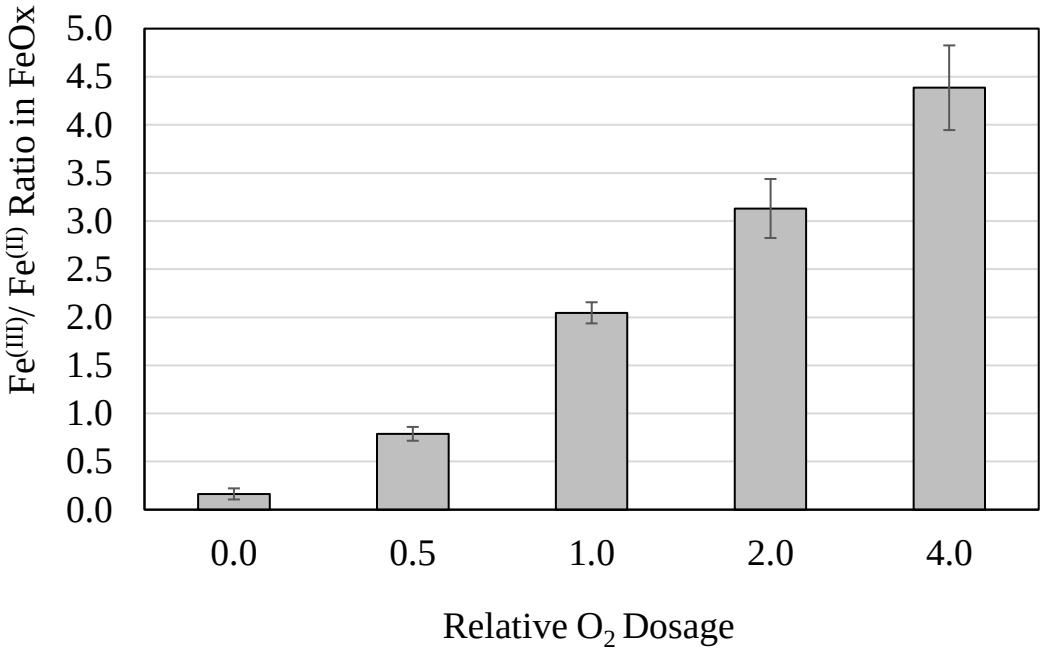


Fig. 4.1. Ratio of $Fe^{(III)}/Fe^{(II)}$ in the $FeO_x$ produced from the oxidation of $Fe(OH)_2$ by $O_2$ as a function of $O_2$ dosage. Initial concentration was same as 0.75 mM $Fe^{2+}$ and 1.55 mM NaOH. Dosage of $O_2$ is expressed in a relative value to the stoichiometric one for magnetite formation under the test condition (0.005 m mol $O_2$).

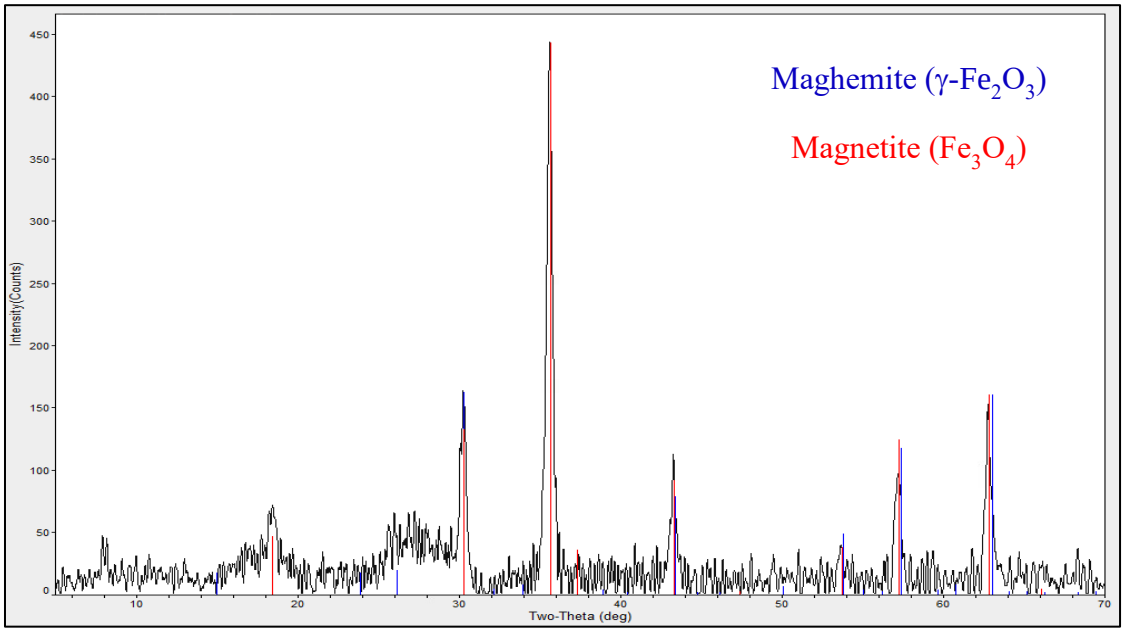


Fig. 4.2. The XRD spectra of the FeOx produced from the oxidation of $Fe(OH)_2$ by $O_2$ under alkaline condition. The spectra match well with that of magnetite (or maghemite), indicating that despite significant $Fe^{(III)}/Fe^{(II)}$ variation, the general structure of FeOx remains an inverse spinel structure that is a characteristic of magnetite.

### 4.1.2 Formation of FeOx by $O_2$ in the presence of ZVI

The test was conducted to evaluate the general method of preparing the activated iron media through an aeration process. The above tests (see section 3.1.1) showed that oxidative precipitation of $Fe(OH)_2$ through careful control of $O_2$ dosage and application rate under alkaline condition could form a desirable FeOx phase with mixed Fe(III)/F(II) ratio and an inverse-spinel structure similar to that of $Fe_3O_4$ (magnetite). In this section, we aim to add ZVI into the process and evaluate (1) if aeration would form a desirable iron oxide coating on the surface of ZVI grain; (2) how the presence of ZVI could affect the dosage of $O_2$ required for forming the desired FeOx.

As described in chapter 2, we conduct a series of batch tests that started with the same initial concentrations of 0.75 mM $Fe^{2+}$ and 1.55 mM NaOH, but with the addition of 10 mg 100 mesh ZVI in the reactor. Similarly, the headspace was filled with varying amounts of $O_2$ dosage in a series of parallel tests. After reaction completed, the resulting ZVI and iron oxides was sampled and analyzed to determine its compositional and structural characteristics.

The change of Fe(III) : Fe(II) ratio produced with the presence of 10 mg ZVI in the reactor is illustrated in Fig. 4.3. Similar to Fig.4.1, the relative dosage of $O_2$ (0.005 m mol) for production of magnetite based on Eq. 4.1 was set as 1. In the test with the presence of ZVI, the ratio of Fe(III) : Fe(II) of FeOx formed upon reaction completed was lower than the ratio obtained under the comparable conditions without ZVI. When 0.0056 m mol $O_2$ was supplied, the ratio of Fe(III) : Fe(II) was 1.38. On the other hand, the stoichiometric ratio of magnetite was shown when 0.012 m mol $O_2$ was provided. This result indicates that additional $O_2$ is needed to maintain the stoichiometric ratio due to the oxidation of ZVI. In the reactor with 0.012 m mol $O_2$, black magnetite coating was observed after 20 h. The result from XRD spectra of the peeled off layer is shown in Fig 4.4.

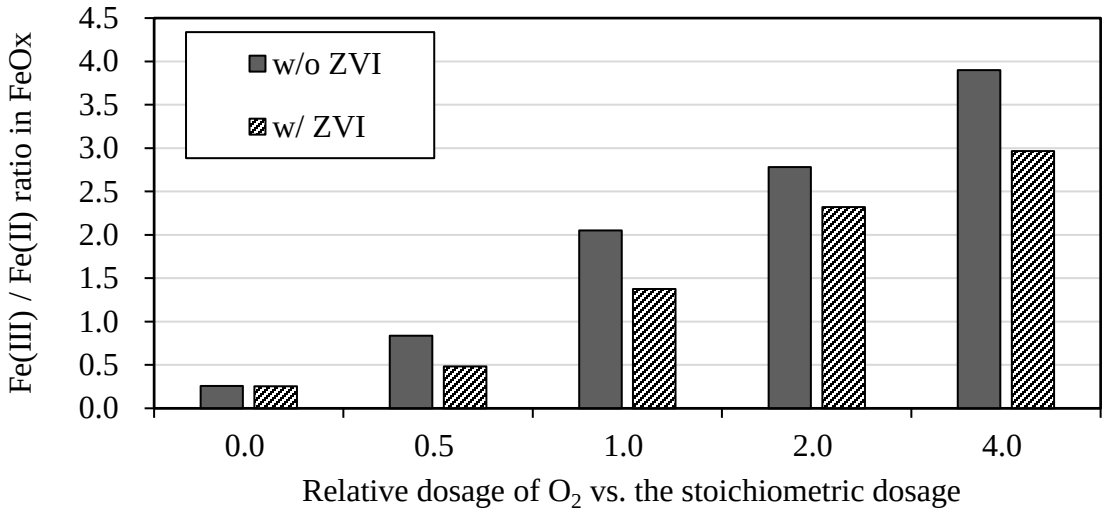


Fig. 4.3. Change of Fe(III)/Fe(II) ratio in the FeOx product formed through oxidation of $Fe(OH)_2$ by $O_2$ in the presence vs absence of ZVI as a function of $O_2$ dosage. The initial concentrations were: 0.75 mM $Fe^{2+}$, 1.55 mM NaOH and 10 mg 100 mesh ZVI. The stoichiometric dosage of $O_2$ of 1.0 corresponds to 0.0056 m mol $O_2$ supply.

Figure 4.3 showed that with the presence of ZVI, the oxidative precipitation of $Fe(OH)_2$ by $O_2$ would result in a lower ratio of Fe(III)/Fe(II) in the FeOx product. Some of the $O_2$ introduced into the reactive system could be consumed by ZVI, which could form an iron oxide coating on the ZVI grain surface. With less $O_2$ available to oxidize $Fe(OH)_2$, the end product of FeOx would contain less Fe(III) and thus the ratio of Fe(III)/Fe(II) would be lowered than the one without ZVI of the same $O_2$ dosage. The implication here is that with the presence of ZVI, more $O_2$ would be needed than the stoichiometric dosage in order to form a FeOx with target ratio of Fe(III)/Fe(II), e.g., formation of ideal magnetite crystalline with an ideal ratio of Fe(III)/Fe(II) =2.

(1) FeOx still formed with the presence of ZVI in the $Fe(OH)_2/O_2$ system; The structure still possesses characteristic of magnetite; (2) Increased dosage of $O_2$ still

increase the Fe(III)/Fe(II) ratio in the formed iron oxide crystalline. With the presence of ZVI, however, the same desired Fe(III)/Fe(II) ratio would require a high dosage of $O_2$; (3) Some $O_2$ appears to be consumed by ZVI corrosion process, which forms an iron oxide coating on the surface and contributes to the increased dosage of required $O_2$. Overall, the test showed that $O_2$ aeration could be a viable method to convert ZVI + $Fe^{2+}$ system into an activated iron media system with a right recipe and under controlled chemical conditions.

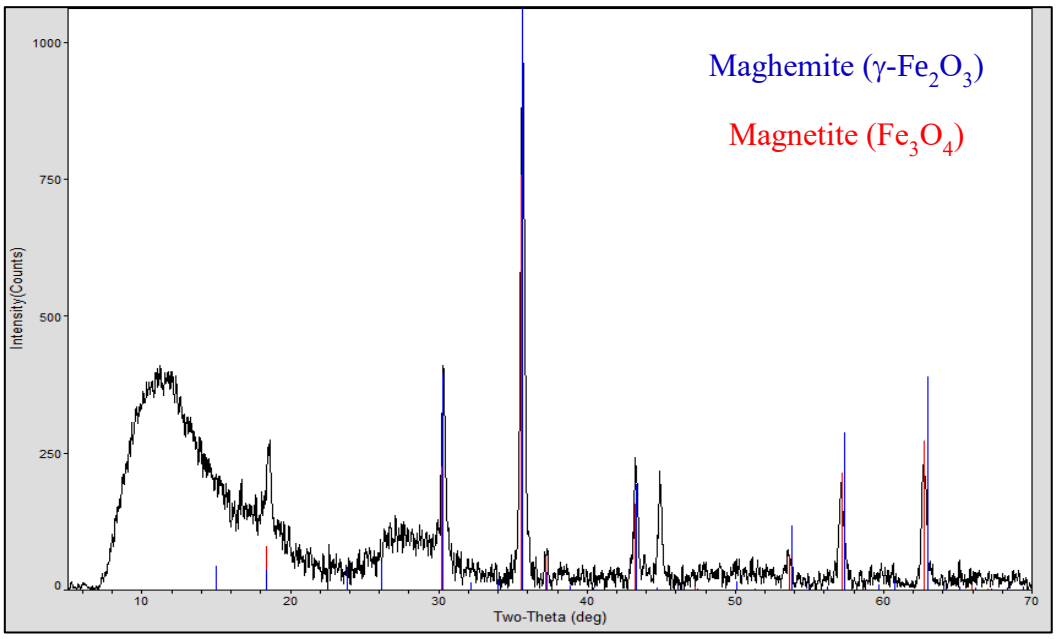


Fig. 4.4. The XRD spectra of the pilled off FeOx layer on the surface of ZVI. The spectra match well with that of magnetite (or maghemite), indicating that despite significant $Fe^{(III)}/Fe^{(II)}$ variation, the general structure of FeOx remains an inverse spinel structure that is a characteristic of magnetite.

The test results demonstrate that aeration of a mixture of $Fe^{2+}$ and ZVI powder under the right conditions such as pH, alkalinity, aeration intensity, and duration could result in the formation of a discrete FeOx with desirable Fe(III)/Fe(II) ratio as well as

formation of an iron oxide coating on ZVI surface. It could be inferred that the iron oxide coating on the ZVI surface could share a similar structure and composition of Fe(III)/Fe(II) with that of the discrete FeOx formed from the oxidation of $Fe(OH)_2$.

4.1.3 Pilot scale production of the activated iron media using aeration method

As a scaled up test to demonstrate feasibility of the new media preparation method, 200 L reactor was used to prepare the activated iron media. The reactor was filled with 200 L tap water; 2.88 kg $FeSO_4.7H_2O$ salt was added into the reactor. The mixer was turned on to dissolve $FeSO_4$ salt. 0.822 kg of NaOH was then added into the reactor, which dissolved quickly and reacted with $Fe^{2+}$ to form $Fe(OH)_2$ precipitate. NaOH was slightly overdosed, which was to ensure the reactant mixture has an initial alkaline condition with a pH of about 11. 2 kg of ZVI (5 um size) was then added. The aeration pump was then turned on and the flow rate was regulated through a needle valve to provide a designed air flow rate of 11 L/min. The mixture in the reactor would react quickly. The key reaction is the oxidation of $Fe(OH)_2$ to become FeOx, which was accompanied with a color change from a slightly-oxidized, greenish $Fe(OH)_2$ floc precipitate to become dark greenish and then black precipitate. In the meantime, pH also decreased from 11 to 9. After 5 hr aeration and reaction (Fig 4.5.), the $Fe(OH)_2$ floc was transformed into magnetite-dominated FeOx crystalline that features strong magnetic property and settles fast . The ZVI grain surface was found to covered by a black coating, presumably a highly reactive magnetite-like iron oxide surface.

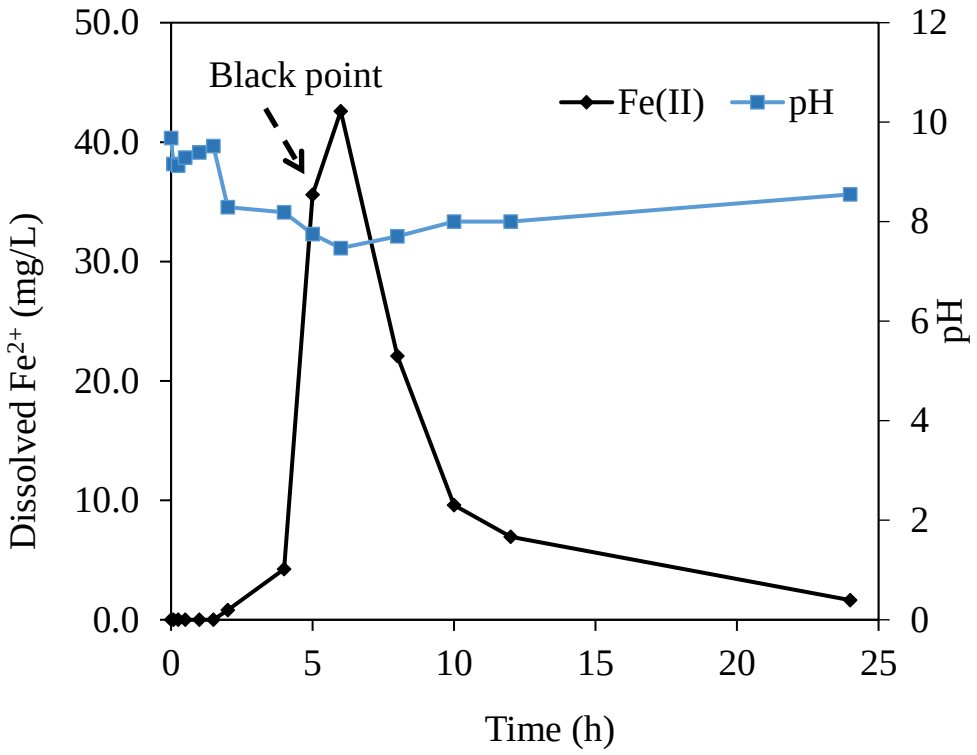


Fig. 4.5. Change of dissolved $Fe^{2+}$ and pH over time during the pilot-scale preparation of the activated iron media in 200 L reactor tank. The recipe for preparation was: 822 g NaOH, 2 kg 5 µm ZVI, 2.88 kg $FeSO_4.5H_2O$, 11 L/min aeration (Data was provided by the courtesy of Dr. Lin XU)

## 4.2 Removal of Sb(V) by the Activated Iron Media

### 4.2.1 Effect of AIM dosage on Sb(V) removal

The tests were conducted to evaluate Sb(V) removal efficiency as a function of the dosage of the activated iron media and the contact time .

As described in Chapter 2, we conduct a series of batch tests that started with the same initial Sb(V) concentration of 50 mg/L, but with varying dosage of AIM. The dosage of the Activated Iron Media was increased from 10 g/L to 50 g/L. After selected time intervals, the reactant mixture were sampled and filtered. The filtrate was analyzed for dissolved Sb(V) to construct a time course for the removal of Sb(V) with different dosages of ZVI.

The results of Sb(V) removal with the different activated iron media dosages are shown in Fig. 4.6. The results showed that Sb(V) removal has three stages. In the first stage, rapid Sb(V) removal was observed from 5 min to 30 min. From 30 min to 4 h, the removal efficiency increased much more slowly, which constitutes the second stage. After 4 h, Sb(V) removal efficiency was mostly stagnant or increased only slightly.

An equilibrium of Sb(V) removal was observed at 4 h in this study. Even though small difference was founded after 4 h, it can be acceptable as experimental error. At the equilibrium, the Sb(V) removal efficiency of 10 g/L of AIM was 52%. The removal efficiency of equilibrium was increased by 66%, 85%, and 99% when the AIM dosage increased to 20 g/L, 30 g/L, and 40 g/L respectively. However, a negligible enhancement was observed when the AIM dosage increased more than 40 g/L.

(1) Sb(V) removal process under anaerobic condition can be associated with surface adsorption due to insignificant enhancement after saturation at a certain time. (2) Initial rapid Sb(V) removal can be related to the available adsorption sites and chemisorption in the initial phase.

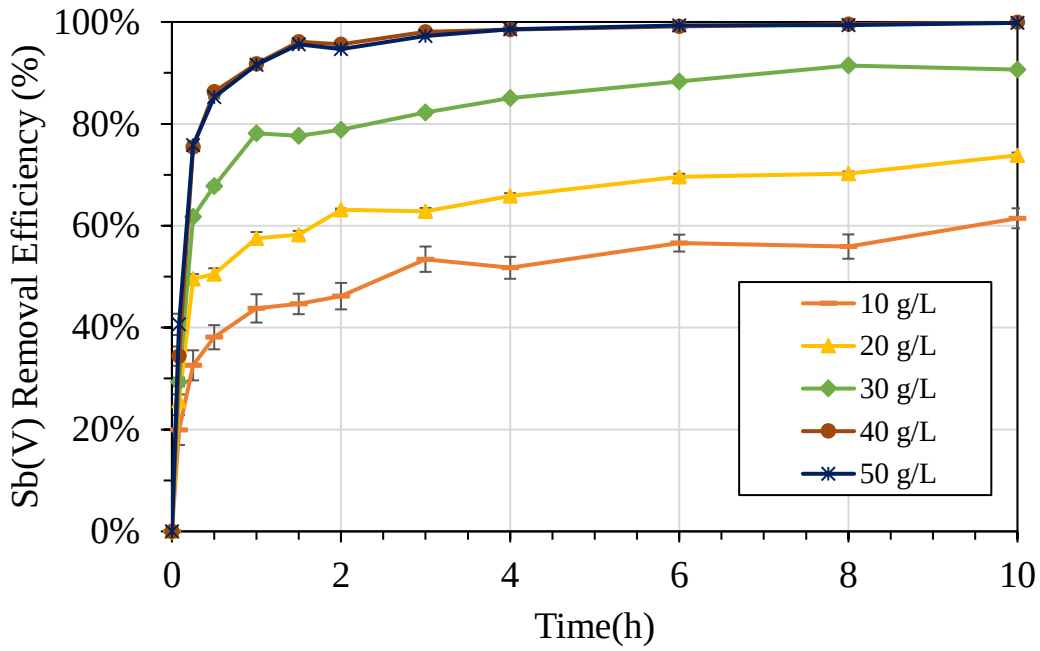


Fig. 4.6. Effect of the activated iron media dosages (10-50 g/L) on Sb(V) removal in anaerobic condition. Initial Sb(V) concentration was 50 mg/L. Reactors were mixed for 10 h at 30 rpm and room temperature. Error bars represent standard deviation (n=3).

4.2.2 Effect of dissolved $Fe^{2+}$ on Sb(V) removal by AIM

The test was conducted to evaluate the effect of aqueous $Fe^{2+}$ on Sb(V) removal by the activated iron media. The above test (section 3.2.1) illustrated that Sb(V) removal through varying dosages of AIM. In this section, we introduce aqueous $Fe^{2+}$ in the activated iron media system for treating Sb(V) and evaluate how aqueous $Fe^{2+}$ would affect Sb(V) removal by the AIM over time.

As described in Chapter 2, we conduct a series of batch tests that started with the same initial Sb(V) concentration of 50 mg /L and the AIM dosage of 10-50 g/L, but with externally supplied aqueous $Fe^{2+}$ of 0.5 mM. At selected reaction time intervals, the reactant mixture were sample and filtered. The filtrate were analyzed for dissolved $Fe^{2+}$, pH and Sb(V) to evaluate the removal efficiency.

Externally added $Fe^{2+}$ was known to play a key role in overcoming surface passivation of ZVI and maintaining its high reactivity for contaminant removal such as nitrate removal (Huang et al 2003) and selenate removal (Tang et al. 2016). In fact, dissolved $Fe^{2+}$ (and its surface adsorption form) is considered to be an essential component of the activated iron media.

As shown in Fig. 4.7., Sb(V) removal efficiency increased greatly in the AIM/$Fe^{2+}$system. In the absence of aqueous $Fe^{2+}$, Sb(V) removal in AIM (10 g/L) system, could not achieve ~65% even at 10 h. When 0.5 mM $Fe^{2+}$ was provided, removal efficiency was substantially enhanced, and it reached 65% in 30 min only. At the equilibrium, the Sb(V) removal efficiency of 10 g/L of AIM/$Fe^{2+}$system was 79%. As the dosage of AIM increased, the removal efficiency was promoted; at the media dosage

of 30 g/L, virtually a complete removal of Sb(V) was achieved by 30 min (Fig.4.7). In contrast, only 68% removal was achieved in the comparable test without adding $Fe^{2+}$ (Fig. 4.6).

(1) The aqueous $Fe^{2+}$ played an important role in Sb(V) removal by the activated iron media system. (2) Adsorbed aqueous $Fe^{2+}$ might facilitate the adsorption and removal of Sb(V) by the activated iron media through the formation of reactive sites on FeOx coating on ZVI. The dosage of $Fe^{2+}$ on the system performance was not evaluated and the fate of the added $Fe^{2+}$ was not monitored. Therefore, the tests here alone was not sufficient to decode the role of the added $Fe^{2+}$.

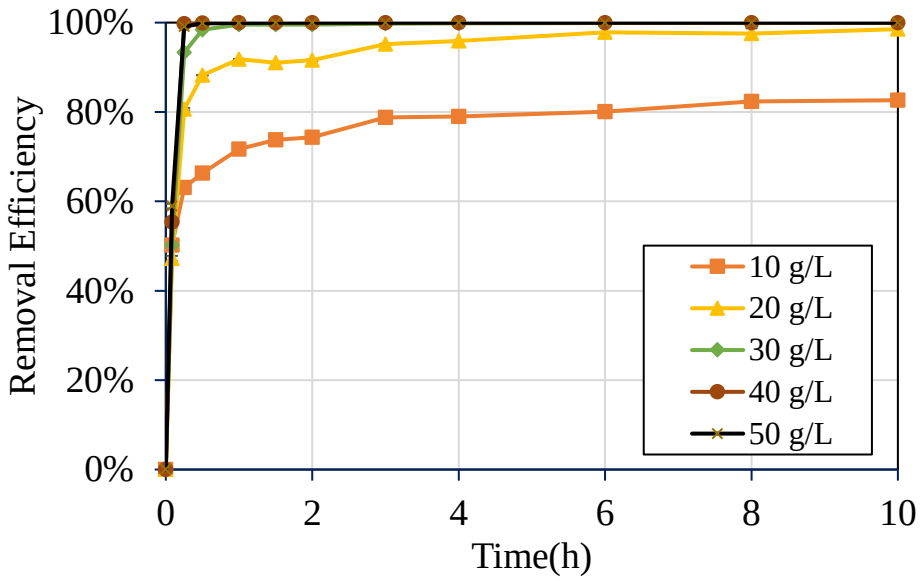


Fig. 4.7. Sb(V) removal in the activated iron system augmented with externally added 0.5 mM $Fe^{2+}$. The initial conditions were: 10-50 g/L media + 50 mg/L Sb(V) + 0.5 mM $Fe^{2+}$. Error bars represent standard deviation (n=3).

4.2.3 Enhanced Sb(V) Removal by AIM with $O_2$ supply

The tests were conducted to evaluate how the presence of $O_2$ would affect Sb(V) removal by the activated iron media with or without externally added $Fe^{2+}$. The above test (Section 3.2.2) demonstrated that Sb(V) removal by the AIM system could be promoted by externally added $Fe^{2+}$. Our goal in this section is to evaluate if aeration would be synergic for the Sb(V) removal.

According to the Chapter 2, a series of batch tests was conducted in serum bottle with the identical initial concentrations as 50 mg /L of Sb(V) and 10 g/L of AIM, but with or without externally added $Fe^{2+}$ (0.5 mM) and $O_2$ dosage (inject 1.0 mL air per hour to the reactor headspace). At the specific reaction time, the reactant mixture were sampled and filtered. The filtrate were analyzed for dissolved $Fe^{2+}$, pH and Sb(V) to evaluate system performance.

The externally supplied $O_2$ was reported to enhance the removal efficiency of contaminants, such as perchlorate, dyes, Cr(VI), enhanced as the increase of the concentration of $O_2$ (Wang et al., 2010; Im et al., 2011; Yoon et al., 2011a). Guo et al. (2015, 2016) also reported that the presence of strong oxidants could facilitate the intense oxidation of the surface of the ZVI. Dissolved $O_2$ was found to accelerate iron corrosion in the presence of dissolved $Fe^{2+}$ (Huang and Zhang, 2005).

As shown in Fig. 4.8a, at the equilibrium, the Sb(V) removal efficiency for the AIM and the AIM/$Fe^{2+}$ systems were enhanced significantly when $O_2$ was supplied to the AIM treatment system. In 15 min, Sb(V) removal efficiency in the AIM/$Fe^{2+}$ system was 63%. In contrast, Sb(V) was removed almost completely (99.9%) in the

AIM/$Fe^{2+}$/$O_2$ system within 15 min. After 30 min, the concentration of Sb(V) was below the EPA permissible Sb concentrations in drinking water as (6 μg/L). This result indicate that $O_2$ can greatly enhance Sb(V) removal efficiency in the AIM system.

The measured pH is given in Fig. 4.8b. Rapid pH change was observed in 15 min coupled with the significant removal of Sb(V) in Fig. 4.8a. In the AIM and the AIM/$O_2$ system the pH increase was observed in 15 min, however, the pH decreased in a short amount time with the presence of aqueous $Fe^{2+}$. After 15 min, all systems maintained the pH until 10 h.

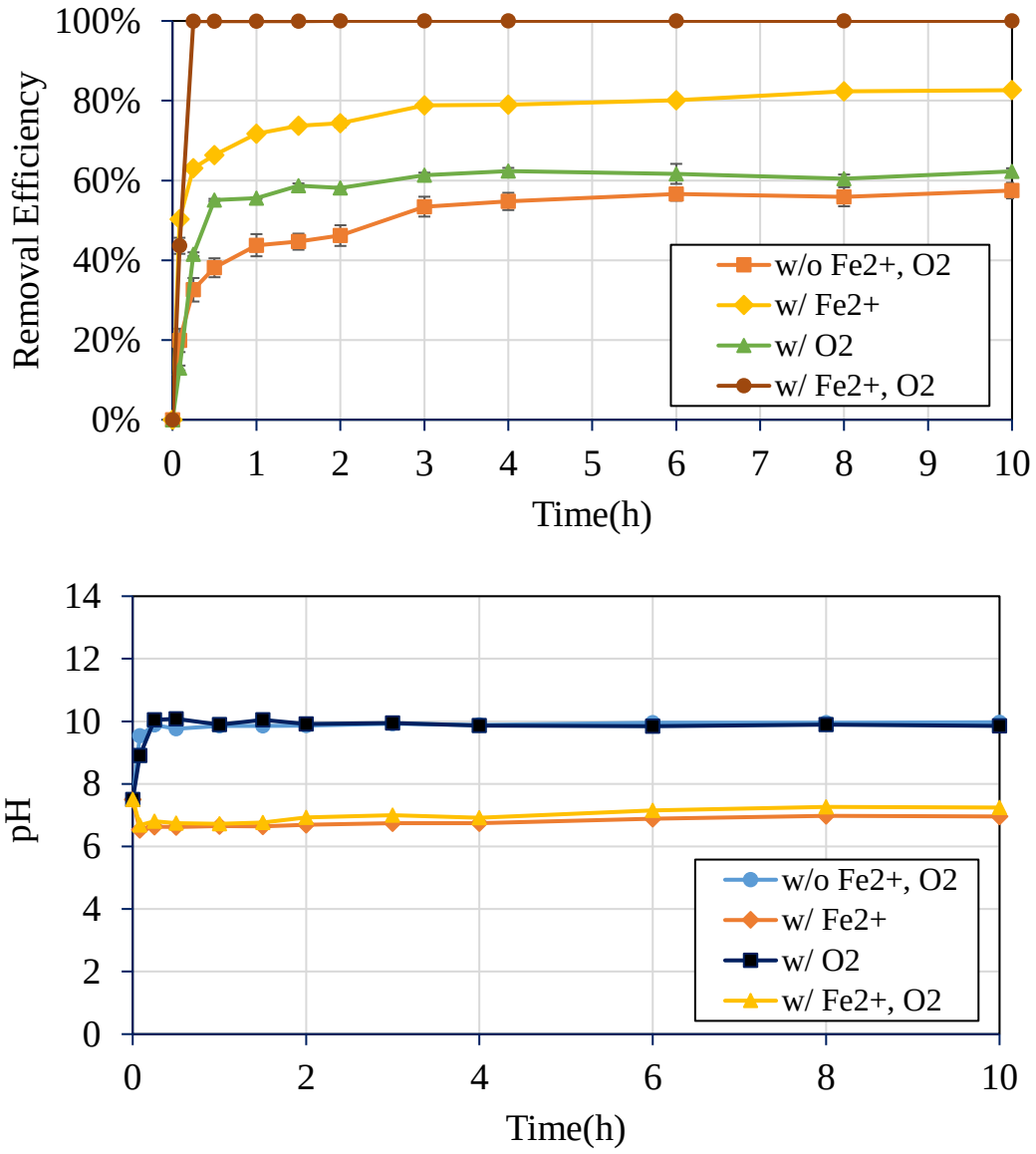


Fig. 4.8. Time-course profiles of (a) Sb(V) removal efficiency and (b) pH change in the activated iron media treatment system with or without externally supplied $Fe^{2+}$ and $O_2$. The initial test concentration was identical as 50 mg/L of Sb(V) and 10 g/L of AIM. 0.5 mM aqueous $Fe^{2+}$ was externally supplied and $O_2$ was spiked at 1 mL/h aeration. Error bars represent standard deviation (n=3).

(1) The supplied $O_2$ may promote formation of FeOx on the surface that can be additional available adsorption site for Sb(V). (2) The supplied aqueous $Fe^{2+}$ would serve as a buffer in the AIM system. In 2016, similar results were reported during the selenate removal with the absence of aqueous $Fe^{2+}$ (Tang et al., 2016). (3) Dissolved Sb(V) might be stabilized by incorporating into the formed FeOx layer on the surface. Overall, the test indicates that the optimum condition for Sb(V) removal is AIM/$Fe^{2+}$/$O_2$ and AIM system could be a desirable method to remove Sb(V) in aerobic condition with neutral pH level.

4.2.4 Statistical analysis for enhanced Sb(V) removal

The analysis was conducted to evaluate the difference between the four different conditions at equilibrium. In order to verify the result from section 3.23, one way analysis of variance analysis was conducted with 95% of confidence interval. The probability value(α) was less than 0.05. Thus, the null hypothesis could be rejected so that the difference between four levels could be an alternative hypothesis. Threshold in table 4.1 indicates lower value at the 95% of confidence interval. In this table, the significance level is more than 0.05 in between all group. Although mean value of each condition has significant difference, the difference between AIM and AIM with $O_2$ was minimum and the difference between AIM and AIM with aqueous $Fe^{2+}$ and $O_2$ was maximum which agrees with the result in Figure 4.8a. Based on the Tukey-Kramer HSD Test, the connecting letters report is shown in Figure 4.9. The test in each condition were triplicated.

| | **w/ $Fe^{2+}$, $O_2$** | **w/ $Fe^{2+}$** | **w/ $O_2$** | **w/o $Fe^{2+}$, $O_2$** |
|---|---|---|---|---|
| w/ $Fe^{2+}$, $O_2$ | -0.02958 | 0.17719 | 0.35049 | 0.43376 |
| w/ $Fe^{2+}$ | 0.17719 | -0.02958 | 0.14372 | 0.22699 |
| w/ $O_2$ | 0.35049 | 0.14372 | -0.02958 | 0.05369 |
| w/o $Fe^{2+}$, $O_2$ | 0.43376 | 0.22699 | 0.05369 | -0.02958 |

Table 4.1. Tukey-Kramer HSD Threshold Matrix for enhanced Sb(V) removal. Confidence interval was 95%. Positive values show pairs of means that are significantly different.

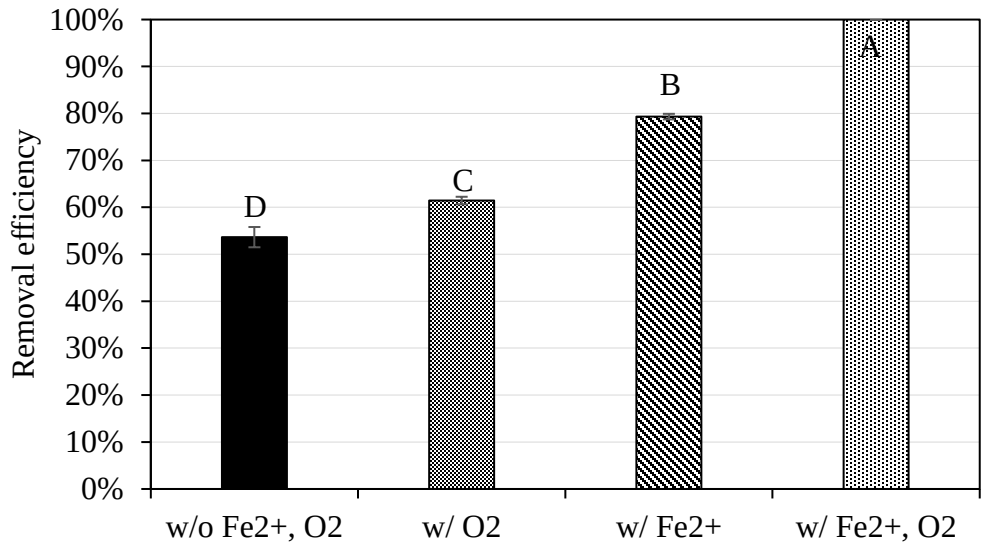


Fig. 4.9. Sb(V) removal efficiency of different systems at equilibrium. Error bar represent standard deviation (n=3). Connecting letters represent the relevance within each system. Different letters in this figure indicate significant statistical differences ($P < 0.05$) according to the Tukey-Kramer HSD test.

### 4.3 Characterization of the kinetics of Sb(V) adsorption

4.3.1 Pseudo reaction model for Sb(V) removal

Kinetics of Sb(V) adsorption was characterized by applying the pseudo reaction models (Lagergren, 1898; Ho an McKay, 1999). Equations below were employed in this study.

$$\ln[q_e - q_t] = \ln[q_e] - k_1 t/2.303 \quad \text{eq. 4.2}$$

$$\frac{t}{q_t} = \frac{1}{k_2 (q_e)^2} + \frac{t}{(q_e)} \quad \text{eq. 4.3}$$

In this equation, the $q_e$ is the theoretical adsorption capacity of the equilibrium. When time is t (min), $q_t$ is the amount of adsorbed Sb(V) on the surface of AIM and $k_1$(/min), $k_2$(mg/g min) is the equilibrium rate constants of 1st and 2nd reaction model respectively.

In table 4.2., all parameters of pseudo 1st and 2nd order reaction model are shown. As the higher correlation coefficient $R^2$ indicates, all conditions were fitted better to the pseudo 2nd reaction model (Fig. 4.10). Similar results were reported on the Sb(V) adsorption reaction (Li et al., 2012; Liu et al., 2015; Wang et al., 2012). The theoretical adsorption capacity qe was similar with the experimental value also indicate the suitability of pseudo 2nd order reaction model. The highest theoretical adsorption capacity ($q_e$ = 5.09) was observed under the condition of $O_2$ and $Fe^{2+}$. Other $q_e$ values from AIM, AIM/$O_2$, and AIM/$Fe^{2+}$were 2.73 mg/g, 3.27 mg/g, and 3.74 mg/g respectively. The $q_e$ value from the adsorption conditions with the existence of $O_2$ was higher than the adsorption conditions without $O_2$. A similar role of $O_2$ was observed during adsorption of arsenate (Yang et al., 2017). During the selenate removal test in 2016, the rate constant also dramatically increased when the $Fe^{2+}$was introduced (Tang

et al., 2016). This result demonstrated $Fe^{2+}$can enhance the adsorption of Sb(V) under oxic condition.

| Condition | $q_e$ (mg/g) | Pseudo 1st order | | |
|---|---|---|---|---|
| | | $q_e$ (mg/g) | $k_1$ | $R^2$ |
| w/o $Fe^{2+}$, $O_2$ | 2.68 | 0.2 | 0.0139 | 0.884 |
| w/ $Fe^{2+}$ | 3.77 | 0.158 | 0.0364 | 0.948 |
| w/ $O_2$ | 3.11 | 0.12 | 0.0181 | 0.850 |
| w/ $Fe^{2+}$, $O_2$ | 5.00 | 0.004 | 0.11 | 0.421 |
| Condition | $q_e$ (mg/g) | Pseudo 2nd order | | |
| | | $q_e$ (mg/g) | $k_2$ | $R^2$ |
| w/o $Fe^{2+}$, $O_2$ | 2.68 | 2.73 | 0.303 | 0.990 |
| w/ $Fe^{2+}$ | 3.77 | 3.74 | 0.161 | 0.997 |
| w/ $O_2$ | 3.11 | 3.27 | 0.211 | 0.995 |
| w/ $Fe^{2+}$, $O_2$ | 5.00 | 5.09 | 0.087 | 0.999 |

Table 4.2. Parameters of Pseudo 1st and 2nd order reaction for Sb(V) adsorption, at room temperature under four conditions reaction. Initial conditon: 50 mg/L of Sb(V), 10 g/L AIM, $O_2$ (1 mL/h aeration), 0.5 mM aqueous $Fe^{2+}$.

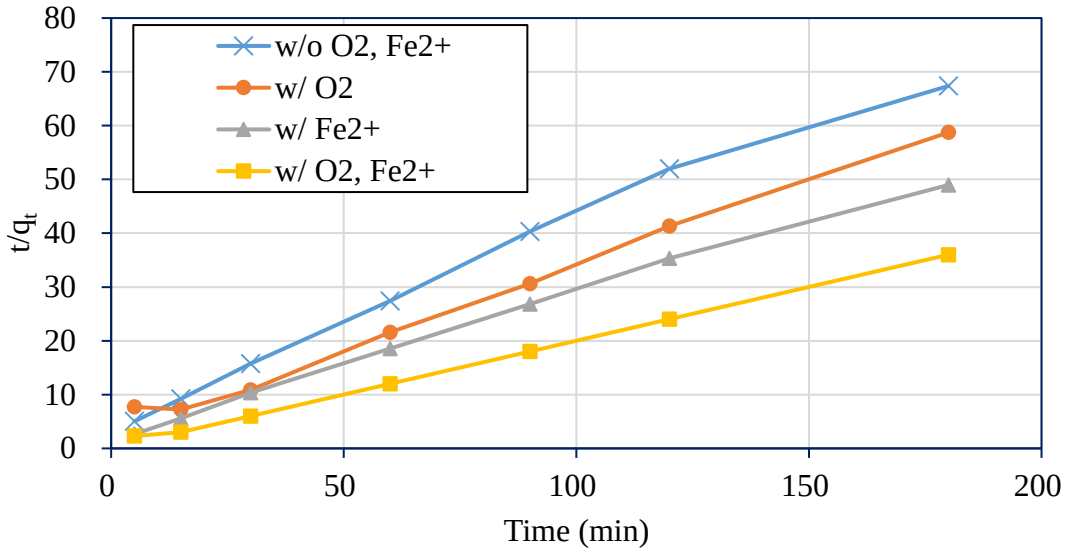


Fig. 4.10. Pseudo 2nd order reaction model. Initial conditon: 50 mg/L of Sb(V), 10 g/L AIM, $O_2$ (1 mL/h aeration), 0.5 mM aqueous $Fe^{2+}$.

4.3.2 Langmuir and Freundlich isotherms

Two isotherm (Langmuir, Freundlich) models were applied to fit the data in this study (Fig. 4.11, Fig.4.12). The initial concentration of Sb(V) ranged from 50 to 200 mg/L at pH 7.5 and at 298 K. These two simple models are commonly used to characterize the adsorption of liquid phase components on to the solid adsorbent (Xi et al., 2010). When the surface of the adsorbent is a monolayer, Langmuir model will be applied. When the surface of the adsorbent is heterogeneous, Freundlich model will be applied (Yoon et al., 2016). Freundlich isotherm model is shown below equation 4.4.

$$q_e = K{C_e}^{1/n} \qquad \text{eq. 4.4}$$

In eq. 4.4, when $C_e$ (mg/L) is the concentration of adsorbate at equilibrium, $q_e$ (mg/g) is the amount of adsorbed Sb on the adsorbent. The Freundlich constant for adsorption

capacity is K and the adsorption intensity is 1/n. The Landmuir isotherm model is expressed in eq. 4.5.

$$q_e = \frac{q_0 b C_e}{1 + b C_e} \qquad \text{eq. 4.5}$$

In equation 4.5, $C_e$ and $q_e$ are same as the previous definition, and $b$ is a constant for finding strength and $q_0$ (mg/g) is the maximum adsorption capacity. These equations can be linearized to generate the parameter from the empirical data.

$$\frac{Ce}{q_e} = \frac{1}{q_0 b} + \frac{Ce}{q_0} \qquad \text{eq. 4.6}$$

$$\ln qe = \ln K + 1/n \cdot \ln Ce \quad \text{eq.4.7}$$

Data from Sb(V) adsorption test are shown in Table 4.3. In anaerobic conditions, both of Langmuir and Freundlich model fit well ($R^2$ = 0.99). Similar trends were observed in previous studies (Wang et al., 2012; Xi et al., 2010). On the other hand, when $O_2$ was introduced, the adsorption model tends to perform slightly less then anaerobic conditions in Freundlich model. Similar trends were also observed from Langmuir model, which demonstrated that other reaction might occur in AIM/$O_2$, AIM/$Fe^{2+}$/$O_2$ system.

In the AIM/$Fe^{2+}$/$O_2$ system, the higher $R^2$ value of Freundlich model suggests that Sb was adsorbed with forming a heterogeneous layer on the surface. It indicates that the physical and chemical adsorption was occurred simultaneously. On the other hand, during the arsenate adsorption, both anaerobic and oxic condition formed the monolayer (Yang et al., 2017). This result suggests that the adsorption behavior of Sb(V) is different from As(V) on the adsorption under oxic condition. In Freundlich model, the adsorption capacity, K value, was significantly higher at the AIM/$Fe^{2+}$/$O_2$ system.

| Condition | T(°C) | Freundlich constant | | | Langmuir constants | | |
|---|---|---|---|---|---|---|---|
| | | n | K(L/g) | $R^2$ | $q_0$(mg/g) | b(L/mg) | $R^2$ |
| $Fe^{2+}$ | 25 | 1.16 | 0.439 | 0.992 | 63.29 | 0.0051 | 0.997 |
| $O_2$ | 25 | 1.24 | 0.297 | 0.979 | 36.90 | 0.0048 | 0.992 |
| w/o $Fe^{2+}$, $O_2$ | 25 | 1.36 | 0.249 | 0.999 | 14.22 | 0.0091 | 0.994 |
| w/ $Fe^{2+}$, $O_2$ | 25 | 7.15 | 12.182 | 0.919 | 10.62 | 235.5 | 0.85 |

Table 4.3. Parameters of Freundlich and Langmuir model for adsorption of Sb (V) by different conditions. Initial conditon: 50 mg/L of Sb(V), 10 g/L AIM, $O_2$ (1 mL/h aeration), 0.5 mM aqueous $Fe^{2+}$. Reaction time was 4 h.

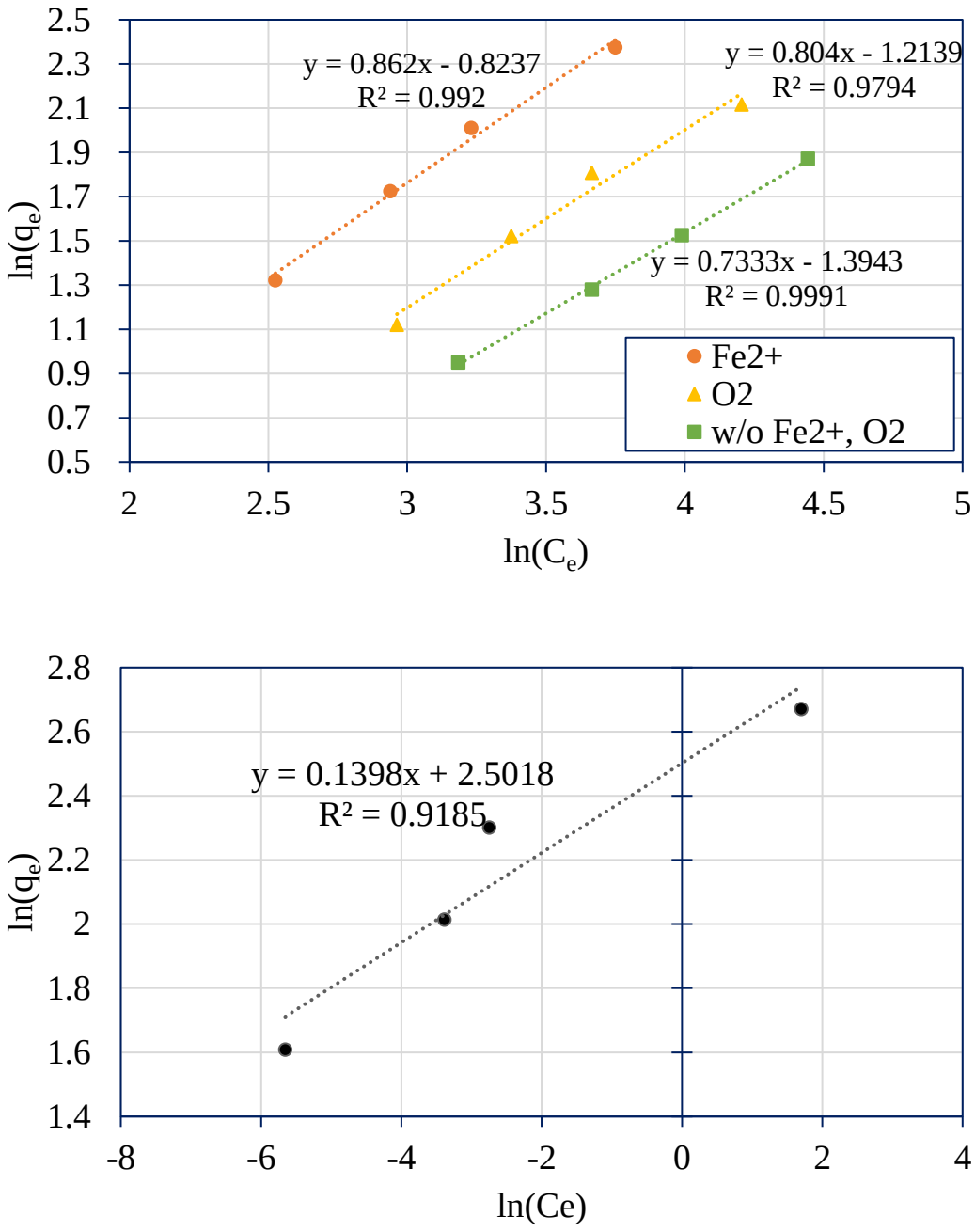


Fig. 4.11. Freundlich isotherm for Sb(V) adsorption on different conditions. Initial conditon: 50 mg/L of Sb(V), 10 g/L AIM, $O_2$ (1 mL/h aeration), 0.5 mM aqueous $Fe^{2+}$. Reaction time was 4 h.

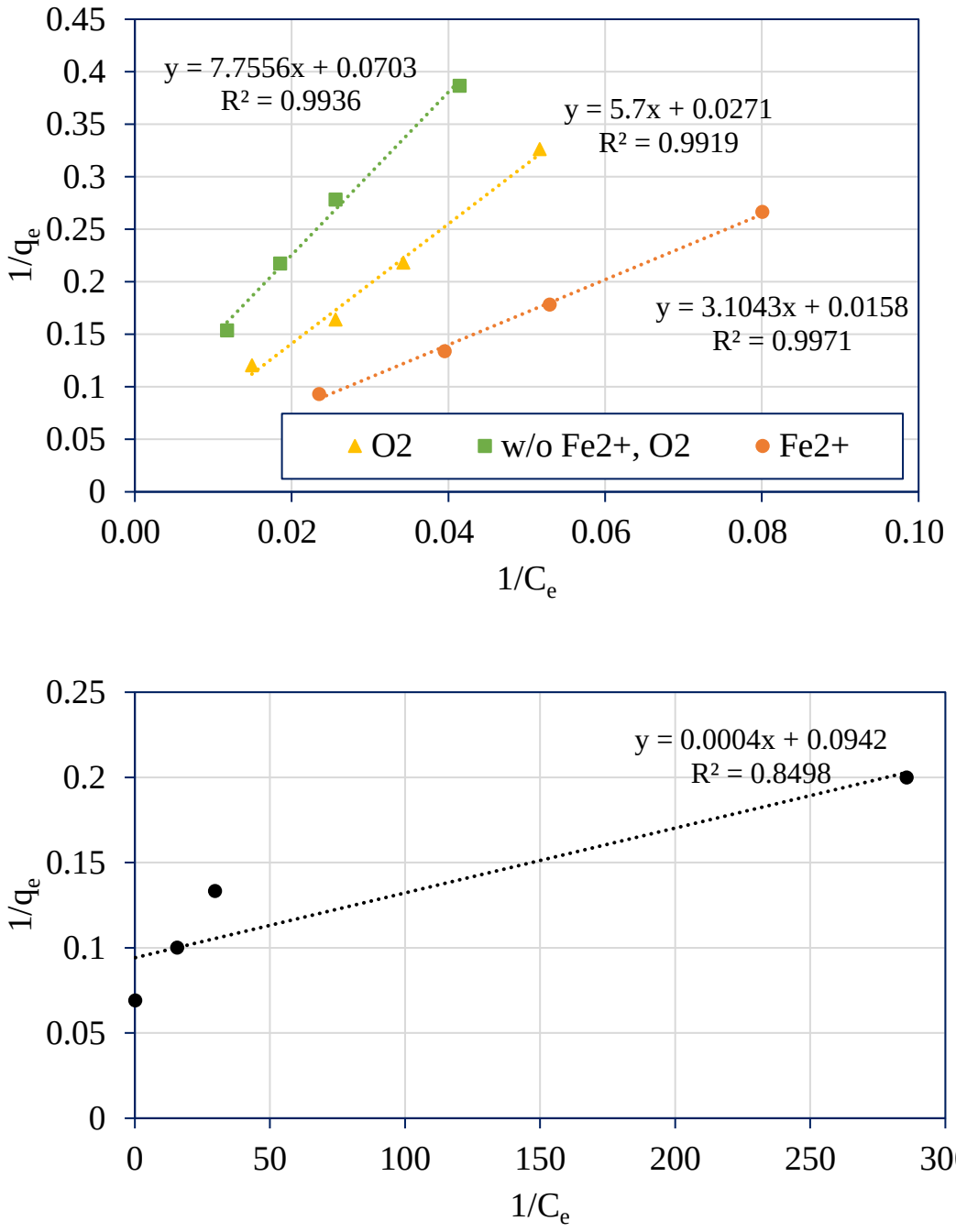


Fig. 4.12. Langmuir isotherm for Sb(V) adsorption on different conditions. Initial conditon: 50 mg/L of Sb(V), 10 g/L AIM, $O_2$ (1 mL/h aeration), 0.5 mM aqueous $Fe^{2+}$. Reaction time was 4 h.

### 4.4 pH effects on Sb(V) removal

The test was conducted to examine the effects of pH levels on Sb(V) removal by AIM. The above test (section 3.2.3) illustrated that enhancement of Sb(V) removal through supplying the aqueous $Fe^{2+}$ and $O_2$. In this section, we aim to adjust the initial pH level and evaluate (1) the effect of initial pH level on Sb(V) removal with two different conditions.

As described in chapter 2, we conduct two series of batch tests started with initial concentration as Sb(V) 50 mg /L and AIM 10 g/L; (2) Sb(V) 50 mg /L , AIM 10 g/L, 0.5 mM aqueous $Fe^{2+}$ and $O_2$ aeration 1mL/h. The pH was controlled with the level of 3, 5, 7, 9, and 11 respectively. The reactors were mixed for 4 hours in the rotating tumbler at room temperature and 30 rpm. After the reaction, dissolved $Fe^{2+}$ and Sb(V) in supernatant were sampled and analyzed.

Sb(V) removal could be promoted at low pH level by the promotion of iron corrosion and the dissolution of $FeO_x$ layer which may detrimental of the reacitivy of ZVI (Bae and Lee, 2014; Dong et al., 2010). Another study for Sb(V) removal by using $Fe_3O_4$ observed that the pH level 3-4 was the optimum (Wang et al., 2012; Verbinnen et al., 2013). Similar results were found with other iron-based adsorbents, such as ZVI and hydrous ferric oxide (Guo et al., 2014; Zhang et al., 2007). On the other hand, in the high pH range, ZVI could be passivate, lose the reactivity, due to the $FeO_x$ layer buildup on the surface of ZVI (Noubactep, 2008).

Sb(V) removal at different pH level is illustrated in Fig. 4.13. As the results describe, in the AIM/$Fe^{2+}$/$O_2$ system, substantial Sb(V) removal efficiency was observed

at all pH level. However, the optimum pH range for AIM system without $Fe^{2+}$and $O_2$ was 3. Between the pH range 5 to 9, removal efficiency was decreased to 52% but decreased significantly as 18% at the pH increased 11.

The concentration of the remaining aqueous $Fe^{2+}$ is illustrated in Fig. 4.14. However, when the pH is higher than 3, negligible amount of aqueous $Fe^{2+}$ was detected. At the pH 3, the aqueous $Fe^{2+}$ was higher than externally supplied concentration (0.5 mM). When the initial pH was higher than 3, the final pH was above 9.0 as the result of anaerobic ZVI oxidation. On the other hand, with a low level of pH 3, the final pH was increased to 5.71 coupling with released $Fe^{2+}$. At the pH range 3-9, the AIM/$Fe^{2+}$/$O_2$ system could keep the final pH stable near 6.5.

(1) The difference of Sb(V) adsorption can be associated with the ionic Sb(V) species at different pH level. At the pH range 5-10, Sb(V) can be stabilized as $Sb(OH)_6^-$ (Tella and Porokovski, 2012). On the other hand, because of the competitive adsorption between hydroxyl ions, the adsorption efficiency is likely decreased. (2) The adsorption is possibly associated with pH range at the point of zero charge. When the pH is lower than pH at the point of zero charge, the surface of adsorbents is positively charged. Thus, the adsorption can be promoted by the higher concentration of $H^+$ ions. However, when the pH is higher than pH at the point of zero charge the surface of adsorbents is charged negatively. The increase of Sb(V) removal efficiency might be the same reason. (3) At pH level 3, the ZVI oxdation and dissolution of FeOx surface layer were promoted. Generally, in aerobic conditions, $O_2$ serves as the fianl electron acceptor. On the other

hand, under the anaerobic condition, ZVI can be corrosive with $H_2O$ as an oxidant. The equation below describes the ZVI corrosion.

$$Fe^0 + 2H_2O \rightarrow Fe^{2+} + 2OH^- + H_2\uparrow \quad \text{eq 4.8}$$

On the other hand, with a low level of pH 3, hydrogen serves as an electron acceptor and ZVI can be oxidized (equation 4.9).

$$Fe^0 + 2H^+ \rightarrow Fe^{2+} + H_2\uparrow \quad \text{eq 4.9}$$

(4) Morover, although the aqueous $Fe^{2+}$ would serve as a buffer in the AIM system, the resulting pH still remains acidic condition. Thus, employment for wastewater treatment may not applicable in acidic condition.

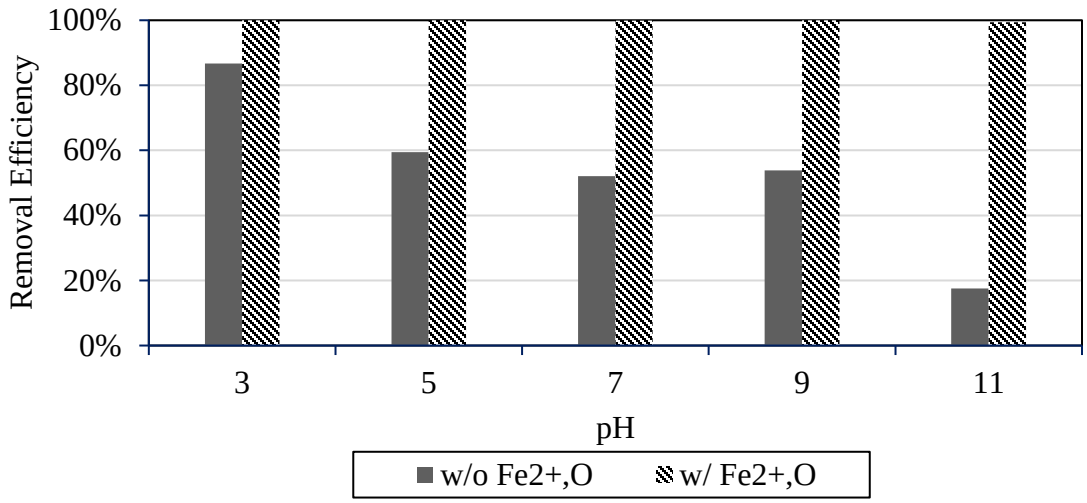


Fig. 4.13. pH effect on Sb(V) removal. Initial concentration was 50 mg/L of Sb(V) and 10 mg/L of AIM. Reaction time was 4 h at 30 rpm and room temperature. Extenally additive was 0.5 mM $Fe^{2+}$ and 1 mL/h aeration of $O_2$.

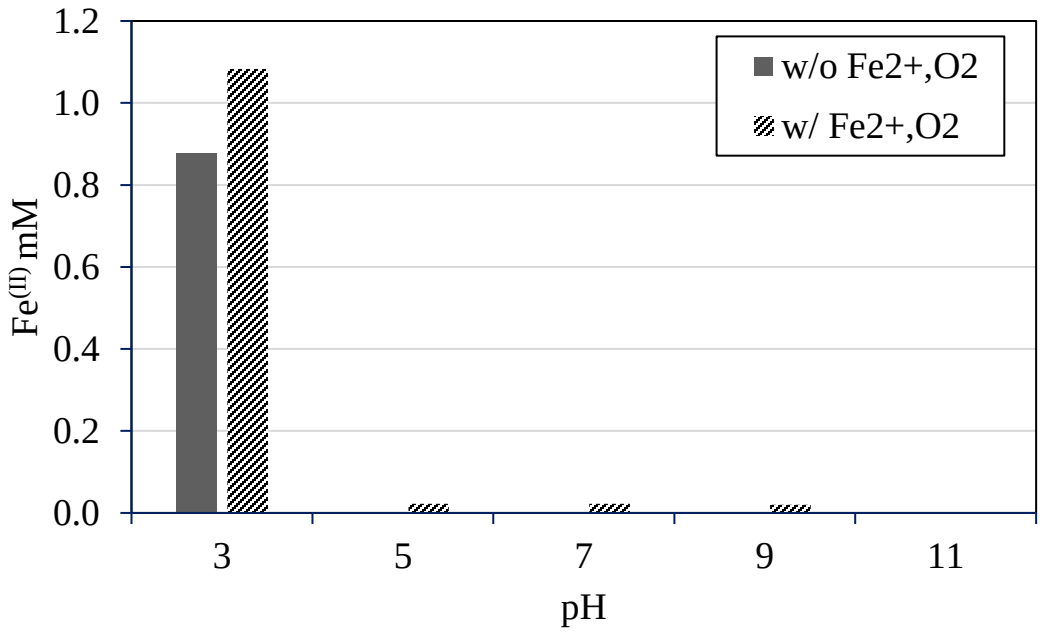


Fig. 4.14. Concentration of dissolved $Fe^{2+}$after Sb(V) removal. Initial concentration was 50 mg/L of Sb(V) and 10 mg/L of AIM. Reaction time was 4 h at 30 rpm, room temperature. 0.5 mM $Fe^{2+}$ and 1 mL/h of $O_2$ was externally supplied.

### 4.5 Sequential dosing experiment

The test was conducted to elucidate the role of Fe(II) in the AIM/Fe(II) system. The above test (section 3.2.2) demonstrated that the Sb(V) removal was promoted by externally added $Fe^{2+}$ on AIM. In this section, our goal is to evaluate (1) if the supplied aqueous $Fe^{2+}$ would enhance the ZVI and AIM system; (2) how the dosage of aqueous $Fe^{2+}$ would affect the Sb(V) removal efficiency.

According to the chapter 2, a series of batch tests was conducted with the identical initial concentrations as 50 mg /L of Sb(V), but with varying the dosages of added aqueous $Fe^{2+}$. At specific time intervals, another dosage of 50 mg/L Sb(V) and

specific dosage of aqueous $Fe^{2+}$ were added. The pH and the dissolved Sb(V) in supernatant was sampled and analyzed to evaluate the removal efficiency.

The crucial role of externally supplied aqueous $Fe^{2+}$ in anaerobic condition was reported in previous studies (Tamaura et al., 1983; Huang et al., 2006; Huang et al., 2012). Due to the buildup of ferric (oxyhydro)oxides layers on the surface, ZVI could be passivated. The externally supplied aqueous $Fe^{2+}$ could be adsorbed on the surface of ZVI. The ferric (oxyhydro)oxides layer could converted by adsorbed $Fe^{2+}$ to magnetite. A previous study demonstrated the magnetite could be oxidized to $r$-$Fe_2O_3$, but externally supplied aqueous $Fe^{2+}$ converted $r$-$Fe_2O_3$ to magnetite (Huang and Zhang, 2005).

The results of Sb(V) removal from a sequential dosing experiment are shown in Fig.4.15a. As shown, Sb(V) removal was coupled with the consumption of dissolved $Fe^{2+}$ (Fig. 4.15b). A first dosage of 50 mg/L Sb(V) was removed in 1.5 h in the AIM system. However, the removal efficiency of Sb(V) at ZVI system was less than 50% at 2 h. When the externally supplied $Fe^{2+}$ was present at the second dosage of 50 mg/L Sb(V), the removal efficiency was significantly increased. This result indicates that the aqueous $Fe^{2+}$ plays an important role in Sb(V) removal, which was consistent with the role of aqueous $Fe^{2+}$ in Fig. 4.8a. Similar result was reported at the selenate removal (Tang et al., 2016).

In the absence of aqueous $Fe^{2+}$, Sb(V) concentration in the AIM/$Fe^{2+}$ system decreased below μg/L level after 1h. When 0.3 mM $Fe^{2+}$ was supplied, negligible enhancement was observed. On the other hand, when $Fe^{2+}$ dosage was increased to 0.5

mM, the Sb(V) removal rate was improved signinficantly, and it only took 30 m to remove dissolved Sb(V) to μg/L levels. A further dosage of externally supplied $Fe^{2+}$ increased to 0.8 mM, but the enhancement of Sb(V) removal was negligible. Some residual $Fe^{2+}$ was detected in the ZVI/$Fe^{2+}$ and the AIM/$Fe^{2+}$ systems when $Fe^{2+}$ dosage was increased to 0.5 mM. Once the significant initial removal occurred in 15 m, further consumption of dissolved $Fe^{2+}$ was not substaintial until the 3$^{rd}$ dosage. The removal efficiency of Sb(V) from the 3$^{rd}$ dosage increased as the aqueous $Fe^{2+}$ was consumed.

(1) The surface coated FeOx layer play a crucial role of promoting Sb(V) removal efficiency. Similar roles of magetite was observed during nitrate reduction, molybate removal and selenate removal (Huang et al., 2012; Xu et al., 2012; Tang et al., 2016). (2) The externally supplied aqueous $Fe^{2+}$ consumped rapidely coupled with Sb(V) removal. This aqueous $Fe^{2+}$ may rejuvenate the reactivity of ZVI and form additional $FeO_x$ layers on the surface. (3) The Sb(V) removal in 3$^{rd}$ dosage was not rapid as 2$^{nd}$ dosage because of not enough time to form the FeOx layer on the surface. Overall test indicates the Sb(V) removal consume the externally added $Fe^{2+}$ which contibute the formation of additional FeOx layer that promote Sb(V) removal.

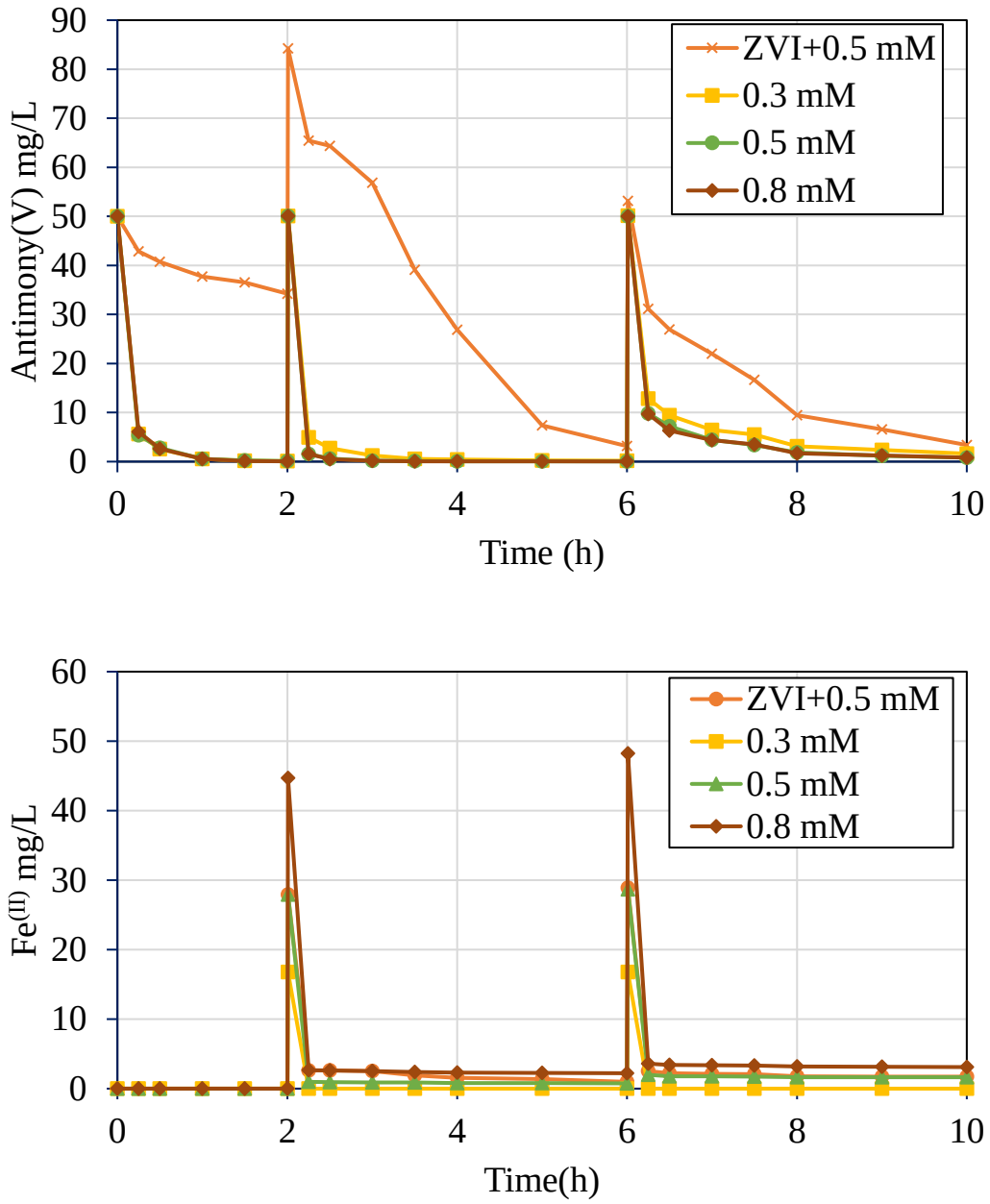


Fig. 4.15. Profiles of (a) dissolved Sb(V) and (b) dissolved $Fe^{2+}$in sequential dosing experiment. The concentration of Sb(V) at each dosage was 50 mg/L. Initial concentration of ZVI and AIM was 50 g/L. Reaction time was 4 h at 30 rpm and room temperature.

# CHAPTER V

## SUMMARY

The Activated Iron Media (AIM) system is a desirable technology to treat the heavy metal remediation from industrial wastewater. In this study, we investigate how externally supplied $O_2$ from aeration would form a discrete FeOx coating on the surface of ZVI and evaluate the AIM reactivity and performance to remove Sb(V) in water. For this purpose, batch tests were conducted to form the FeOx layer on the surface of ZVI and perform the AIM system treatment. The results show that with a stoichiometric dosage of $O_2$/Fe(II) at 1 : 6, magnetite ($Fe_3O_4$) was produced as precipitation of $Fe(OH)_2$ by $O_2$, which was corroborated by a ratio of Fe(III)/Fe(II) at 2:1 as well as an inverse-spinel structure identified by X-ray diffraction (XRD) spectroscopy.

However, with the presence of ZVI, the consumption externally supplied $O_2$ could be promoted, which resulted in a lower Fe(III) contribution in FeOx coating. The surface of the ZVI was corroded and formed FeOx layer similar to the precipitates from oxidation of $Fe(OH)_2$. When the $O_2$ dosage increased to double, the Fe(III)/Fe(II) ratio in the resulting FeOx was near 2.3 : 1, close to the desired ratio of magnetite. The result of scaled-up pilot test showed appropriate dosage and intensity of $O_2$ aeration, the mixture of ZVI and $Fe^{2+}$ with controlled alkalinity could be converted to form a mixture of highly reactive media with a magnetite-like FeOx in the form of a coating on ZVI or discrete crystalline.

The result of the batch tests using the Activated Iron Media to treat Sb-contaminated water revealed the three (initial rapid, secondary negligible enhanced and

stationary) phase. The initial phase revealed rapid removal within the first 15 min, followed by a slower phase before entering a stagnant phase, which could be better modelled as a chemisorption. Both externally supplied $O_2$ and $Fe^{2+}$ would somewhat help Sb(V) removal by the AIM, but with the co-presence of $O_2$ and $Fe^{2+}$, Sb(V) removal by the AIM could be greatly enhanced, in which a treatment of 50 mg/L with 10 g/L AIM could decrease Sb(V) to below 6 μg/L in 15 min. Even the Sb(V) removal efficiency was high at an acidic pH condition, and concentration of the aqueous $Fe^{2+}$ was higher than the initial due to the iron corrosion. Sequential dosing test that such high removal of Sb(V) could be sustained in a continuous flow treatment system. For a remediation of Sb(V), AIM treatment should be operated with aeration and externally supplied aqueous $Fe^{2+}$.

This study further elucidate the knowledge and methods to form AIM system and extend its potential application scope to cover wastewater with elevated Sb(V) concentration.

## REFERENCES


Agrawal, A., & Tratnyek, P. G. (1995). Reduction of nitro aromatic compounds by zero-valent iron metal. *Environmental Science & Technology*, *30*(1), 153-160.

Bae, S., & Lee, W. (2014). Influence of riboflavin on nanoscale zero-valent iron reactivity during the degradation of carbon tetrachloride. *Environmental science & technology*, *48*(4), 2368-2376.

Belzile, N., Chen, Y. W., & Wang, Z. (2001). Oxidation of antimony (III) by amorphous iron and manganese oxyhydroxides. *Chemical Geology*, *174*(4), 379-387.

Blandamer, M. J., Burgess, J., & Peacock, R. D. (1974). Solubility of sodium hexahydroxoantimonate in water and in mixed aqueous solvents. *Journal of the Chemical Society, Dalton Transactions*, (10), 1084-1086.

Blowes, D. W., Ptacek, C. J., & Jambor, J. L. (1997). In-situ remediation of Cr (VI)-contaminated groundwater using permeable reactive walls: laboratory studies. *Environmental Science & Technology*, *31*(12), 3348-3357.

Boller, M. A., & Steiner, M. (2002). Diffuse emission and control of copper in urban surface runoff. *Water Science and Technology*, *46*(6-7), 173-181.

Choe, S., Chang, Y. Y., Hwang, K. Y., & Khim, J. (2000). Kinetics of reductive denitrification by nanoscale zero-valent iron. *Chemosphere*, *41*(8), 1307-1311.

Dang, F., Kamada, K., Enomoto, N., Hojo, J., & Enpuku, K. (2007). Sonochemical synthesis of the magnetite nanoparticles in aqueous solution. *Journal of the Ceramic Society of Japan*, *115*(1348), 867-872.

Deng, R. J., Jin, C. S., Ren, B. Z., Hou, B. L., & Hursthouse, A. S. (2017). The Potential for the Treatment of Antimony-Containing Wastewater by Iron-Based Adsorbents. *Water*, *9*(10), 794.

Diemar, G. A., Filella, M., Leverett, P., & Williams, P. A. (2009). Dispersion of antimony from oxidizing ore deposits. *Pure and Applied Chemistry*, *81*(9), 1547-1553.

Dai, C., Zhou, Z., Zhou, X., & Zhang, Y. (2014). Removal of Sb (III) and Sb (V) from aqueous solutions using nZVI. *Water, Air, & Soil Pollution*, *225*(1), 1799.

Dong, J., Zhao, Y., Zhao, R., & Zhou, R. (2010). Effects of pH and particle size on kinetics of nitrobenzene reduction by zero-valent iron. *Journal of environmental sciences*, *22*(11), 1741-1747.

Elleouet, C., Quentel, F., Madec, C. –L., & Filella, M. (2005). The effect of the presence of trace metals on the oxidation of Sb(III) by hydrogen peroxide in aqueous solution. *Journal of Environmental Monitoring*, *7*(12), 1220–5.

Ettler, V., Mihaljevič, M., Šebek, O., & Nechutný, Z. (2007). Antimony availability in highly polluted soils and sediments–a comparison of single extractions. *Chemosphere*, *68*(3), 455-463.

Filella, M., Belzile, N., & Chen, Y. W. (2002). Antimony in the environment: a review focused on natural waters: I. Occurrence. *Earth-Science Reviews*, *57*(1-2), 125-176.

Filella, M., & May, P. M. (2003). Computer simulation of the low-molecular-weight inorganic species distribution of antimony (III) and antimony (V) in natural waters. *Geochimica et Cosmochimica Acta, 67*(21), 4013-4031.

Filella, M., & May, P. M. (2005). Critical appraisal of available thermodynamic data for the complexation of antimony (III) and antimony (V) by low molecular mass organic ligands. *Journal of Environmental Monitoring*, *7*(12), 1226-1237.

Fu, F., Dionysiou, D. D., & Liu, H. (2014). The use of zero-valent iron for groundwater remediation and wastewater treatment: a review. Journal of hazardous materials, 267, 194-205.

Fu, Z., Wu, F., Mo, C., Liu, B., Zhu, J., Deng, Q., Liao, H., & Zhang, Y. (2011). Bioaccumulation of antimony, arsenic, and mercury in the vicinities of a large antimony mine, China. *Microchemical Journal*, *97*(1), 12-19.

Furukawa, Y., Kim, J. W., Watkins, J., & Wilkin, R. T. (2002). Formation of ferrihydrite and associated iron corrosion products in permeable reactive barriers of zero-valent iron. *Environmental Science & Technology*, *36*(24), 5469-5475.

Gate, S.H., Richardson, E., 1961a. Some studies on antimonic acid I. Some properties, effect of H2O2, and reaction with polyhydroxy compounds. *Journal of Inorganic Nuclear Chemistry*. 23, 257 – 263.

Gayer, K. H., & Garrett, A. B. (1952). The equilibria of antimonous oxide (rhombic) in dilute solutions of hydrochloric acid and sodium hydroxide at 25. *Journal of the American Chemical Society, 74*(9), 2353-2354.

Giasuddin, A. B., Kanel, S. R., & Choi, H. (2007). Adsorption of humic acid onto nanoscale zerovalent iron and its effect on arsenic removal. *Environmental Science & Technology*, *41*(6), 2022-2027.

Gillham, R. W., & O'Hannesin, S. F. (1994). Enhanced degradation of halogenated aliphatics by zero-valent iron. *Groundwater*, *32*(6), 958-967.

Groth, D. H., Stettler, L. E., Burg, J. R., Busey, W. M., Grant, G. C., & Wong, L. (1986). Carcinogenic effects of antimony trioxide and antimony ore concentrate in rats. *Journal of Toxicology and Environmental Health, Part A Current Issues*, *18*(4), 607-626.

Guan, X., Sun, Y., Qin, H., Li, J., Lo, I. M., He, D., & Dong, H. (2015). The limitations of applying zero-valent iron technology in contaminants sequestration and the corresponding countermeasures: the development in zero-valent iron technology in the last two decades (1994–2014). *Water research*, *75*, 224-248.

Guo, X., Wu, Z., & He, M. (2009). Removal of antimony (V) and antimony (III) from drinking water by coagulation–flocculation–sedimentation (CFS). *Water research*, *43*(17), 4327-4335.

Guo, X., Wu, Z., He, M., Meng, X., Jin, X., Qiu, N., & Zhang, J. (2014). Adsorption of antimony onto iron oxyhydroxides: adsorption behavior and surface structure. *Journal of hazardous materials*, *276*, 339-345.

Guo, X., Yang, Z., Liu, H., Lv, X., Tu, Q., Ren, Q., ... & Jing, C. (2015). Common oxidants activate the reactivity of zero-valent iron (ZVI) and hence remarkably enhance nitrate reduction from water. *Separation and Purification Technology*, *146*, 227-234.

Guo, X., Yang, Z., Dong, H., Guan, X., Ren, Q., Lv, X., & Jin, X. (2016). Simple combination of oxidants with zero-valent-iron (ZVI) achieved very rapid and highly efficient removal of heavy metals from water. *Water research*, *88*, 671-680.

He, M. (2007). Distribution and phytoavailability of antimony at an antimony mining and smelting area, Hunan, China. *Environmental Geochemistry and Health*, *29*(3), 209-219.

Helz, G. R., Valerio, M. S., & Capps, N. E. (2002). Antimony speciation in alkaline sulfide solutions: role of zerovalent sulfur. *Environmental Science & Technology*, *36*(5), 943–8.

Herath, I., Vithanage, M., & Bundschuh, J. (2017). Antimony as a global dilemma: Geochemistry, mobility, fate and transport. *Environmental pollution*, *223*, 545-559.

Ho, Y. S., & McKay, G. (1999). Pseudo-second order model for sorption processes. *Process biochemistry*, *34*(5), 451-465.

Huang, Y. H., Zhang, T. C., Shea, P. J., & Comfort, S. D. (2003). Effects of oxide coating and selected cations on nitrate reduction by iron metal. *Journal of Environmental Quality*, *32*(4), 1306-1315.

Huang, Y. H., & Zhang, T. C. (2005). Effects of dissolved oxygen on formation of corrosion products and concomitant oxygen and nitrate reduction in zero-valent iron systems with or without aqueous Fe2+. *Water Research*, *39*(9), 1751-1760.

Huang, Y. H., & Zhang, T. C. (2006). Nitrite reduction and formation of corrosion coatings in zerovalent iron systems. *Chemosphere*, *64*(6), 937-943.

Huang, Y. H., Tang, C., & Zeng, H. (2012). Removing molybdate from water using a hybridized zero-valent iron/magnetite/Fe (II) treatment system. *Chemical Engineering Journal*, *200*, 257-263.

Huang, Y. H., Peddi, P. K., Zeng, H., Tang, C. L., & Teng, X. (2013). Pilot-scale demonstration of the hybrid zero-valent iron process for treating flue-gas-desulfurization wastewater: Part I. *Water Science and Technology*, *67*(1), 16-23.

Huang, Y. H., Peddi, P. K., Tang, C., Zeng, H., & Teng, X. (2013). Hybrid zero-valent iron process for removing heavy metals and nitrate from flue-gas-desulfurization wastewater. *Separation and Purification Technology*, *118*, 690-698.

Im, J. K., Son, H. S., & Zoh, K. D. (2011). Perchlorate removal in Fe0/H2O systems: Impact of oxygen availability and UV radiation. *Journal of hazardous materials*, *192*(2), 457-464.

Johnson, C. A., Moench, H., Wersin, P., Kugler, P., & Wenger, C. (2005). Solubility of antimony and other elements in samples taken from shooting ranges. *Journal of environmental quality*, *34*(1), 248-254.

Kang, M., Kawasaki, M., Tamada, S., Kamei, T., & Magara, Y. (2000). Effect of pH on the removal of arsenic and antimony using reverse osmosis membranes. *Desalination*, *131*(1-3), 293-298.

Kang, M., Kamei, T., & Magara, Y. (2003). Comparing polyaluminum chloride and ferric chloride for antimony removal. *Water research*, *37*(17), 4171-4179.

Kolbe, F., Weiss, H., Morgenstern, P., Wennrich, R., Lorenz, W., Schurk, K., ... & Daus, B. (2011). Sorption of aqueous antimony and arsenic species onto akaganeite. *Journal of Colloid and Interface science*, *357*(2), 460-465.

Krupka, K. M., & Serne, R. J. (2002). *Geochemical Factors Affecting the Behavior of Antimony, Cobalt, Europium, Technetium, and Uranium in Vadose Zone Sediments* (No. PNNL-14126). Pacific Northwest National Lab.(PNNL), Richland, WA (United States).

Kiyama, M. (1974). Conditions for the Formation of Fe3O4 by the Air Oxidation of $Fe(OH)_2$ Suspensions. *Bulletin of the chemical society of Japan*, *47*(7), 1646-1650.

Lagergren, S. K. (1898). About the theory of so-called adsorption of soluble substances. *Sven. Vetenskapsakad. Handingarl*, *24*, 1-39.

Lefebvre, J., & Maria, H. (1963). Chimie Minerale-Etude Des Equilibres Dans Les Solutions Recentes De Polyantimoniates. *Comptes Rendus Hebdomadaires Des Seances De L Academie Des Sciences*, *256*(14), 3121.

Leuz, A. –K., & Johnson, C. A. (2005). Oxidation of Sb(III) to Sb(V) by $O_2$ and $H_2O_2$ in aqueous solutions. *Geochimica et Cosmochimica Acta*, *69*(5), 1165–1172

Leuz, A. K., Hug, S. J., Wehrli, B., & Johnson, C. A. (2006). Iron-mediated oxidation of antimony (III) by oxygen and hydrogen peroxide compared to arsenic (III) oxidation. *Environmental science & technology*, *40*(8), 2565-2571.

Leuz, A. K., Mönch, H., & Johnson, C. A. (2006). Sorption of Sb (III) and Sb (V) to goethite: influence on Sb (III) oxidation and mobilization. *Environmental science & technology*, *40*(23), 7277-7282.

Li, J., Bao, H., Xiong, X., Sun, Y., & Guan, X. (2015). Effective Sb (V) immobilization from water by zero-valent iron with weak magnetic field. *Separation and Purification Technology*, *151*, 276-283.

Li, X., Dou, X., & Li, J. (2012). Antimony (V) removal from water by iron-zirconium bimetal oxide: Performance and mechanism. *Journal of Environmental Sciences*, *24*(7), 1197-1203.

Liu, B., Wu, F., Li, X., Fu, Z., Deng, Q., Mo, C., Zhu, J., Zhu, Y., & Liao, H. (2011). Arsenic, antimony and bismuth in human hair from potentially exposed individuals in the vicinity of antimony mines in Southwest China. *Microchemical Journal*, *97*(1), 20-24.

Liu, R., Liu, F., Hu, C., He, Z., Liu, H., & Qu, J. (2015). Simultaneous removal of Cd (II) and Sb (V) by Fe–Mn binary oxide: Positive effects of Cd (II) on Sb (V) adsorption. *Journal of hazardous materials*, *300*, 847-854.

Ilgen, A. G., Majs, F., Barker, A. J., Douglas, T. A., & Trainor, T. P. (2014). Oxidation and mobilization of metallic antimony in aqueous systems with simulated groundwater. *Geochimica et Cosmochimica Acta*, *132*, 16-30.

Luo, J., Song, G., Liu, J., Qian, G., & Xu, Z. P. (2014). Mechanism of enhanced nitrate reduction via micro-electrolysis at the powdered zero-valent iron/activated carbon interface. *Journal of colloid and interface science*, *435*, 21-25.

Mesmer, R. E., & Baes, C. F. (1976). The hydrolysis of cations. *Ed. W i 1 ey, EUA*.

Miao, Y., Han, F., Pan, B., Niu, Y., Nie, G., & Lv, L. (2014). Antimony (V) removal from water by hydrated ferric oxides supported by calcite sand and polymeric anion exchanger. *Journal of environmental sciences*, *26*(2), 307-314.

Mishra, D., & Farrell, J. (2005). Understanding nitrate reactions with zerovalent iron using Tafel analysis and electrochemical impedance spectroscopy. *Environmental science & technology*, *39*(2), 645-650.

Mitsunobu, S., Takahashi, Y., Terada, Y., & Sakata, M. (2010). Antimony (V) incorporation into synthetic ferrihydrite, goethite, and natural iron oxyhydroxides. *Environmental Science & Technology*, *44*(10), 3712-3718.

Navarro, P., & Alguacil, F. J. (2002). Adsorption of antimony and arsenic from a copper electrorefining solution onto activated carbon. *Hydrometallurgy*, *66*(1-3), 101-105.

Nishiyama, S. Y., Saito, K., Saito, K., Sugita, K., Sato, K., Akiba, M., Sairo, T., Tsuendeda, S., Hirota, A., Tamada, M., & Sugo, T. (2003). High-speed recovery of antimony using chelating porous hollow-fiber membrane. *Journal of Membrane Science*, *214*(2), 275-281.

Noubactep, C. (2008). A critical review on the process of contaminant removal in Fe0–$H_2O$ systems. *Environmental technology*, *29*(8), 909-920.

Noubactep, C., Btatkeu, K. B. D., & Tchatchueng, J. B. (2011). Impact of $MnO_2$ on the efficiency of metallic iron for the removal of dissolved CrVI, CuII, MoVI, SbV, UVI and ZnII. *Chemical Engineering Journal*, *178*, 78-84.

Noubactep, C. (2013). Metallic iron for water treatment: A critical review. *Clean–Soil, Air, Water*, *41*(7), 702-710.

O'Carroll, D., Sleep, B., Krol, M., Boparai, H., & Kocur, C. (2013). Nanoscale zero valent iron and bimetallic particles for contaminated site remediation. *Advances in Water Resources*, *51*, 104-122.

Qi, C., Wu, F., Deng, Q., Liu, G., Mo, C., Liu, B., & Zhu, J. (2011). Distribution and accumulation of antimony in plants in the super-large Sb deposit areas, China. *Microchemical Journal*, *97*(1), 44-51.

Quentel, F., & Filella, M. (2002). Determination of inorganic antimony species in seawater by differential pulse anodic stripping voltammetry: stability of the trivalent state. *Analytica Chimica Acta*, *452*(2), 237–244.

Satapanajaru, T., Shea, P. J., Comfort, S. D., & Roh, Y. (2003). Green rust and iron oxide formation influences metolachlor dechlorination during zerovalent iron treatment. *Environmental science & technology*, *37*(22), 5219-5227.

Saito, T., Tsuneda, S., Hirata, A., Nishiyama, S. Y., Saito, K., Saito, K., Sugita, K., Uezu, K., Tamada, M., & Sugo, T. (2004). Removal of Antimony (III) Using Polyol-Ligand-Containing Porous Hollow-Fiber Membranes. *Separation science and technology*, *39*(13), 3011-3022.

Scheinost, A. C., Rossberg, A., Vantelon, D., Xifra, I., Kretzschmar, R., Leuz, A. K., Funke,H., & Johnson, C. A. (2006). Quantitative antimony speciation in shooting-range soils by EXAFS spectroscopy. *Geochimica et Cosmochimica Acta*, *70*(13), 3299-3312.

Shan, C., Ma, Z., & Tong, M. (2014). Efficient removal of trace antimony (III) through adsorption by hematite modified magnetic nanoparticles. *Journal of hazardous materials*, *268*, 229-236.

Shokes, T. E., & Möller, G. (1999). Removal of dissolved heavy metals from acid rock drainage using iron metal. *Environmental Science & Technology*, *33*(2), 282-287.

Shi, J., Ai, Z., & Zhang, L. (2014). Fe@ Fe2O3 core-shell nanowires enhanced Fenton oxidation by accelerating the Fe (III)/Fe (II) cycles. *Water research*, *59*, 145-153.

Smith, R.M., Martell, A.E. (1976). Critical stability constants. In: Inorganic Complexes, vol. 4.

Smith, E. H. (1996). Uptake of heavy metals in batch systems by a recycled iron-bearing material. *Water Research*, *30*(10), 2424-2434.

Tamaura, Y., Ito, K., & Katsura, T. (1983). Transformation of γ-FeO (OH) to $Fe_3O_4$ by adsorption of iron (II) ion on γ-FeO (OH). *Journal of the Chemical Society, Dalton Transactions*, (2), 189-194.

Tang, C., Huang, Y., Zhang, Z., Chen, J., Zeng, H., & Huang, Y. H. (2016). Rapid removal of selenate in a zero-valent iron/Fe3O4/Fe2+ synergetic system. *Applied Catalysis B: Environmental*, *184*, 320-327.

Tella, M., & Pokrovski, G. S. (2012). Stability and structure of pentavalent antimony complexes with aqueous organic ligands. *Chemical Geology*, *292*, 57-68.

Tourky, A. R., & Mousa, A. A. (1948). 150. Studies on some metal electrodes. Part V. The amphoteric properties of antimony tri-and pent-oxide. *Journal of the Chemical Society (Resumed)*, 759-763.

Verbinnen, B., Block, C., Lievens, P., Van Brecht, A., & Vandecasteele, C. (2013). Simultaneous removal of molybdenum, antimony and selenium oxyanions from wastewater by adsorption on supported magnetite. *Waste and Biomass Valorization*, *4*(3), 635-645.

Wang, K. S., Lin, C. L., Wei, M. C., Liang, H. H., Li, H. C., Chang, C. H., Fang, Y. T., & Chang, S. H. (2010). Effects of dissolved oxygen on dye removal by zero-valent iron. *Journal of hazardous materials*, *182*(1-3), 886-895.

Wang, X., He, M., Lin, C., Gao, Y., & Zheng, L. (2012). Antimony (III) oxidation and antimony (V) adsorption reactions on synthetic manganite. *Chemie Der Erde-Geochemistry*, *72*, 41-47.

Wilson, S. C., Lockwood, P. V., Ashley, P. M., & Tighe, M. (2010). The chemistry and behaviour of antimony in the soil environment with comparisons to arsenic: a critical review. *Environmental Pollution*, *158*(5), 1169-1181.

Wu, Z., He, M., Guo, X., & Zhou, R. (2010). Removal of antimony (III) and antimony (V) from drinking water by ferric chloride coagulation: Competing ion effect and the mechanism analysis. *Separation and Purification Technology*, *76*(2), 184-190.

Xi, J., He, M., & Lin, C. (2010). Adsorption of antimony (V) on kaolinite as a function of pH, ionic strength and humic acid. *Environmental Earth Sciences*, *60*(4), 715-722.

Xu, G. M., Shi, Z., & Deng, J. (2006). Removal of antimony from water by iron-oxide coated sand. *ENVIRONMENTAL CHEMISTRY-BEIJING-*, *25*(4), 484.

Xu, W., Wang, H., Liu, R., Zhao, X., & Qu, J. (2011). The mechanism of antimony (III) removal and its reactions on the surfaces of Fe–Mn binary oxide. *Journal of colloid and interface science*, *363*(1), 320-326.

Xu, J., Hao, Z., Xie, C., Lv, X., Yang, Y., & Xu, X. (2012). Promotion effect of Fe2+ and Fe3O4 on nitrate reduction using zero-valent iron. *Desalination*, *284*, 9-13.

Xu, J., Tang, J., Baig, S. A., Lv, X., & Xu, X. (2013). Enhanced dechlorination of 2, 4-dichlorophenol by Pd/FeFe3O4 nanocomposites. *Journal of hazardous materials*, *244*, 628-636.

Yang, Z., Xiu, W., Guo, H., & Li, F. (2017). Arsenate removal from aqueous solution by siderite synthesized under high temperature and high pressure. *Environmental Science and Pollution Research*, *24*(23), 19402-19411.

Yoon, I. H., Bang, S., Chang, J. S., Kim, M. G., & Kim, K. W. (2011). Effects of pH and dissolved oxygen on Cr (VI) removal in Fe (0)/H2O systems. *Journal of Hazardous materials*, *186*(1), 855-862.

Yoon, Y., Park, W. K., Hwang, T. M., Yoon, D. H., Yang, W. S., & Kang, J. W. (2016). Comparative evaluation of magnetite–graphene oxide and magnetite-reduced graphene oxide composite for As (III) and As (V) removal. *Journal of hazardous materials*, *304*, 196-204.

Zhang, D. Y., Pan, X. L., & Song, Y. X. (2009). Removal of antimony from water by zero-valent iron. *Earth and Environment*, *37*(3), 315-318.

Zhang, G., Qu, J., Liu, H., Liu, R., & Wu, R. (2007). Preparation and evaluation of a novel Fe–Mn binary oxide adsorbent for effective arsenite removal. *Water Research*, *41*(9), 1921-1928.

Zhang, T. C., & Huang, Y. H. (2006). Effects of surface-bound Fe 2+ on nitrate reduction and transformation of iron oxide (s) in zero-valent iron systems at near-neutral pH. *Journal of Environmental Engineering*, *132*(5), 527-536.

Zhu, J., Wu, F. C., Deng, Q. J., Shao, S. X., Mo, C. L., Pan, X. L., Li, W., & Zhang, R. Y. (2009). Environmental characteristics of water near the Xikuangshan antimony mine, Hunan Province. *Acta Scientiae Circumstantiae*, *29*(2), 655-661.